



# Angiopoietin-2-Dependent Spatial Vascular Destabilization Promotes T-cell Exclusion and Limits Immunotherapy in Melanoma

Ha-Ram Park<sup>1</sup>, Anahita Shiva<sup>1</sup>, Portia Cummings<sup>1</sup>, Seoyeon Kim<sup>2</sup>, Sungsoo Kim<sup>1</sup>, Eunhyeong Lee<sup>1</sup>, Alessandra Leong<sup>1</sup>, Subrata Chowdhury<sup>1</sup>, Carrie Shawber<sup>3</sup>, Richard Carvajal<sup>4</sup>, Gavin Thurston<sup>5</sup>, Joon-Yong An<sup>2</sup>, Amanda W. Lund<sup>6</sup>, Hee Won Yang<sup>1</sup>, and Minah Kim<sup>1</sup>

## ABSTRACT

T-cell position in the tumor microenvironment determines the probability of target encounter and tumor killing. CD8<sup>+</sup> T-cell exclusion from the tumor parenchyma is associated with poor response to immunotherapy, and yet the biology that underpins this distinct pattern remains unclear. Here we show that the vascular destabilizing factor angiopoietin-2 (ANGPT2) causes compromised vascular integrity in the tumor periphery, leading to impaired T-cell infiltration to the tumor core. The spatial regulation of ANGPT2 in whole tumor cross-sections was analyzed in conjunction with T-cell distribution, vascular integrity, and response to immunotherapy in syngeneic murine melanoma models. T-cell exclusion was associated with ANGPT2 upregulation and elevated vascular leakage at the periphery of human and murine melanomas. Both pharmacologic and genetic blockade of ANGPT2 promoted CD8<sup>+</sup> T-cell infiltration into the tumor core, exerting antitumor effects. Importantly, the

reversal of T-cell exclusion following ANGPT2 blockade not only enhanced response to anti-PD-1 immune checkpoint blockade therapy in immunogenic, therapy-responsive mouse melanomas, but it also rendered nonresponsive tumors susceptible to immunotherapy. Therapeutic response after ANGPT2 blockade, driven by improved CD8<sup>+</sup> T-cell infiltration to the tumor core, coincided with spatial TIE2 signaling activation and increased vascular integrity at the tumor periphery where endothelial expression of adhesion molecules was reduced. These data highlight ANGPT2/TIE2 signaling as a key mediator of T-cell exclusion and a promising target to potentiate immune checkpoint blockade efficacy in melanoma.

**Significance:** ANGPT2 limits the efficacy of immunotherapy by inducing vascular destabilization at the tumor periphery to promote T-cell exclusion.

## Introduction

Melanoma represents the most aggressive form of skin cancer and accounts for the majority of skin cancer-related mortalities (1). Because of its high somatic mutational burden, which is exacerbated by exposure to ultraviolet (UV) radiation, melanoma is highly immunogenic (2). Checkpoint inhibitors, such as those targeting the programmed death-1 (PD-1)/PD-ligand-1 (PD-L1) axis and cytotoxic T-lymphocyte antigen-4 (CTLA4), have demonstrated clinical efficacy with significant increases in the overall survival of patients with metastatic melanoma. In fact, about 70% of patients with advanced melanoma who receive both anti-PD-1 and anti-CTLA4 therapies

show an overall survival rate of 3 years (3–5). Despite these substantial advances in melanoma treatment, 30% to 50% of patients still exhibit *de novo* (primary) resistance to checkpoint inhibitors and an additional 20% to 30% show progression after an initial response (secondary resistance) within 5 years (6). The emergence of resistance is associated with an immunosuppressive tumor microenvironment (TME) characterized by absent or dysfunctional immune cells, including T cells, and has limited therapeutic efficacy in patients. Therefore, elucidating mechanisms underlying a tumor-specific immune evasion is critical to improving immunosuppression and enhancing treatment efficacy in patients with melanoma.

Among potential mechanisms underlying immunosuppression in the TME, T-cell exclusion drives resistance to immunotherapy by sequestering tumor-reactive T cells away from their targets, thereby reducing tumor control (7, 8). Although T-cell exclusion is observed in nonresponsive patients with melanoma as well as other solid tumor types, the signals that drive it remain largely unknown. Emerging evidence suggests that CD8<sup>+</sup> T cells can be excluded from the tumor core by stromal components in the tumor margin, such as the extracellular matrix and inhibitory cytokine production impeding T-cell migration (9, 10). It is known that blood vessels in the TME are abundant, destabilized, and leaky, accompanied by angiogenesis and poor vascular perfusion. Targeting aberrant tumor vasculature with antiangiogenic therapies has shown promise but limited efficacy as a monotherapy. Notably, antiangiogenic tumor therapy targeting vascular endothelial growth factor (VEGF), a prominent proangiogenic molecule, enhanced chemotherapy efficacy in many cancer types (11). This insight suggested that inhibition of angiogenesis causes not only the selective regression of immature blood vessels but also the improvement of remaining vascular function, a process referred to as “vascular normalization” (12). Previous studies also demonstrated that

<sup>1</sup>Department of Pathology and Cell Biology, Columbia University Irving Medical Center, New York, New York. <sup>2</sup>School of Biosystems and Biomedical Sciences, College of Health Science, Korea University, Seoul, Korea. <sup>3</sup>Department of Obstetrics and Gynecology, Columbia University Irving Medical Center, New York, New York. <sup>4</sup>Department of Medicine, Columbia University Irving Medical Center, New York, New York. <sup>5</sup>Regeneron Pharmaceuticals Inc., Tarrytown, New York. <sup>6</sup>Ronald O. Perleman Department of Dermatology, NYU Grossman School of Medicine, NYU Langone Health, New York, New York.

H-R. Park and A. Shiva contributed equally to this article.

**Corresponding Author:** Minah Kim, Pathology and Cell Biology, Columbia University Medical Center, New York, NY 10032. E-mail: mk4242@cumc.columbia.edu

Cancer Res 2023;83:1968–83

**doi:** 10.1158/0008-5472.CAN-22-2838

This open access article is distributed under the Creative Commons Attribution-NonCommercial-NoDerivatives 4.0 International (CC BY-NC-ND 4.0) license.

©2023 The Authors; Published by the American Association for Cancer Research

normalized tumor vasculature through inhibition of VEGF or its receptor (VEGFR-2) promotes extravasation of T cells into the tumor and improves adoptive cell transfer-based immunotherapies in the B16 melanoma model (13). Emerging evidence suggests the importance of normalized blood vessels in facilitating an immunosupportive microenvironment, which is necessary for effective immunotherapy (14, 15). However, the mechanism by which antiangiogenic therapy potentiates the clinical response to immunotherapy remains elusive. Moreover, the role of spatial vascular changes in T-cell exclusion within the tumor is not clearly defined.

ANGPT2, which binds to the receptor tyrosine kinase TIE2 in endothelial cells, is a key regulator of angiogenesis and vascular destabilization. Upregulation of ANGPT2 often correlates with poor prognosis and disease progression in many types of advanced tumors (16–18). Unlike ANGPT2, angiopoietin-1 (ANGPT1) induces activation of TIE2 and promotes vascular maturation and stabilization through the protein kinase Akt, which phosphorylates the forkhead box O1 (FOXO1) transcription factor and thus prevents upregulation of ANGPT2 (19–21). ANGPT2 is released by endothelial cells upon angiogenic or inflammatory stimuli and functions as both an agonist and antagonist of TIE2 in a context-dependent manner (22–24). In pathologic conditions, ANGPT2 competes with ANGPT1 as a TIE2 antagonist, inhibits TIE2 signaling, and promotes FOXO1 transcriptional activity (20, 25–28). Targeting the ANGPT2/TIE2 signaling pathway is suggested to inhibit tumor angiogenesis and growth by interfering with the proangiogenic activity of TIE2-expressing monocytes (TEM; ref. 29). Furthermore, a recent study demonstrated the additive effects of dual targeting VEGF and ANGPT2 on CD8<sup>+</sup> T-cell activation in a B16-OVA melanoma model (30). However, our understanding of how ANGPT2 mechanistically affects tumor immune evasion is incomplete.

In this study, we investigated the mechanistic contribution of ANGPT2/TIE2 signaling to T-cell exclusion. We found that T-cell exclusion was associated with upregulation of ANGPT2 at the tumor periphery in human and mouse melanoma tissues. Both pharmacologic and genetic blockade of ANGPT2 was sufficient to release CD8<sup>+</sup> T cells from the periphery and drive their infiltration to the tumor core, ultimately exerting antitumor effects in syngeneic murine melanomas. Importantly, the reversal of T-cell exclusion following ANGPT2 blockade not only enhanced response to anti-PD-1 in therapy responsive mouse melanomas, but also made nonresponsive tumors susceptible. Mechanistically, therapeutic response after ANGPT2 blockade coincided with spatial TIE2 signaling activation and increased vascular integrity in the tumor periphery. These findings provide novel insights into the mechanistic regulation of ANGPT2-induced T-cell exclusion from the tumor core, highlighting ANGPT2/TIE2 signaling as a promising target to potentiate checkpoint inhibitor efficacy in melanoma.

## Materials and Methods

### Animal models

Pathogen-free C57BL/6J mice were purchased from The Jackson Laboratories. CB17-SCID (C.B-*Igh-1<sup>b</sup>*/IcrTac-*Prkdc<sup>scid</sup>*) mice were purchased from Taconic Biosciences. *Angpt2*<sup>fl/fl</sup> (31, 32) mice were provided by Dr. Gou Young Koh (Korea Advanced Institute of Science and Technology) and bred in Columbia University Irving Medical Center. For conditional endothelial cell-specific targeting of *Angpt2*, we used VE-cadherin-CreER<sup>T2</sup> mice from Dr. Ralf Adams (Max Planck Institute, Munich, Germany; ref. 33). VE-cadherin-CreER<sup>T2</sup> mice were mated with *Angpt2*<sup>fl/fl</sup> mice to generate tamoxifen-induced

endothelial cell-specific *Angpt2*-deleted mice (VE-cadherin-CreER<sup>T2</sup>; *Angpt2*<sup>fl/fl</sup>, termed *Angpt2*<sup>iAEC</sup>). Tamoxifen (2 mg; Sigma-Aldrich, T5648) was injected intraperitoneally for 4 consecutive days beginning at 7 to 8 weeks of age in *Angpt2*<sup>iAEC</sup> mice or wild-type C57BL/6J mice, which were used as a control. Knockout was confirmed using immunofluorescence analysis of tumors for ANGPT2 expression.

Three tumor models (YUMM1.7, YUMMER1.7, B16-F10) were used in this study. B16-F10 cells were purchased from the ATCC. YUMM1.7 (Yale University Mouse Melanoma) and YUMMER1.7 (Yale University Mouse Melanoma Exposed to Radiation) cells harboring driver mutations common in human melanoma (*Braf*<sup>V600E</sup>, *Pten*<sup>-/-</sup>, and *Cdkn2a*<sup>-/-</sup>) were generated by the Bosenberg group at Yale University (34, 35) and were kindly provided by Dr. Amanda Lund at NYU Langone Health (New York, NY; ref. 36). YUMMER1.7 (2.5 × 10<sup>5</sup>), YUMM1.7 (5 × 10<sup>5</sup>), or B16-F10 (1 × 10<sup>5</sup>) cells were subcutaneously inoculated in C57BL/6J, CB17-SCID, or *Angpt2*<sup>iAEC</sup> mice. For pulmonary metastasis, YUMMER1.7 (5 × 10<sup>5</sup>) or B16-F10 (2 × 10<sup>5</sup>, CFP-conjugated or nonconjugated) cells were injected intravenously in C57BL/6J mice. Lungs were collected 3 weeks after cell inoculation. Mice were housed on a 12-hour light/dark cycle with access to food and drinking water in a pathogen-free animal facility. For all experiments, 7- to 8-week-old male mice were used and fed standard chow. All experimental endpoints were studied at 10 to 12 weeks of age unless otherwise specified. Mice were anesthetized by intraperitoneal injection of ketamine (90–100 mg/kg) and xylazine (10–17 mg/kg) before cell inoculation or perfusion. Mice were regularly monitored to follow institutional guidelines for ethical endpoints. All animal experiments were approved by the Institutional Animal Care and Use Committee at Columbia University Irving Medical Center. All experiments followed institutional guidelines for the care and use of laboratory animals.

### Cell culture

Mouse melanoma cell lines YUMMER1.7 and YUMM1.7 were maintained in DMEM/F12 containing 10% FBS. The B16-F10 mouse melanoma cell line was maintained in DMEM containing 10% FBS. All cells were cultured at 37°C and 5% CO<sub>2</sub>. All cell lines tested negative for *Mycoplasma*. All cell lines were maintained under 10 passages and were discarded after use.

### Treatments

Mice were administered 12.5 mg/kg of anti-ANGPT2 antibody (REGN910) or control human IgG antibody (REGN1945) every 3 days (4–5 total doses). Treatment was initiated when tumor volumes were ~70 mm<sup>3</sup>. Subcutaneous tumors were measured twice a week by caliper and collected at perfusion 3 to 4.5 weeks after cell inoculation. For extended treatment, antibodies were administered at the same interval for a total of 10 doses. Mice were euthanized prior to the experimental endpoint if tumor volumes were >2,000 mm<sup>3</sup>. For the CD8<sup>+</sup> T-cell depletion study, either 100 µg/mouse rat IgG or anti-CD8α antibody was administered on days –2 and –1 prior to REGN910 treatment initiation (day 0) once tumor volumes were ~70 mm<sup>3</sup>. Subsequently, anti-CD8α antibodies were administered every 2 days (eight total doses) and REGN910 was administered every 3 days (five total doses). CD8<sup>+</sup> T-cell depletion was confirmed using immunofluorescence analysis of tumors for CD8<sup>+</sup> T-cell expression. For the PD-1 inhibition, mice were administered 100 µg/mouse anti-PD-1 or rat IgG every 2 days (six to seven total doses). Combination treatment consisted of REGN910 every 3 days, concurrent with anti-PD-1 treatment every 2 days. Antibodies are detailed in Supplementary Table S1.

### Tissue preparation and IHC

Mice were perfused with fixative (1% paraformaldehyde in 1× PBS; pH 7.4) through the left ventricle into the aorta for 2 minutes at a pressure of 120 to 140 mmHg. Tumor tissues were collected and fixed with 1% paraformaldehyde for 1 hour on ice and were stored overnight in 30% sucrose at 4°C. Tumors were embedded in optimal cutting temperature compound and cut into 50 μm sections. Sections were rinsed with 1× PBS containing 0.3% Triton X-100 (PBST) and blocked with 5% donkey serum (Jackson ImmunoResearch) for 1 hour at room temperature and then incubated in blocking solution overnight with primary antibodies described in Supplementary Table S2. Slides were incubated with Alexa-labeled secondary antibodies in PBST for 4 hours at room temperature. Nuclei were stained with DAPI (1 mg/mL; Sigma-Aldrich, D9542) for 10 minutes at room temperature and mounted in Vectashield medium (Vector Laboratories).

### Flow cytometry

After tumor collection, we dissected the tumor core and periphery. Each tumor region was minced using razor blades followed by dissociation into single-cell suspensions after placement in digestion medium: FACS buffer (1× PBS containing 2% FBS), 0.1% collagenase IV (Worthington, LS004188), and 10 U/mL DNase type I (Sigma, D4527-20KU). Minced tumors were incubated for 20 minutes at 37°C with constant shaking. Cell suspensions were filtered using a cell strainer (70 μm) to remove cell clumps. Red blood cells (RBC) were lysed using incubating cell suspensions inside RBC lysis buffer (eBioscience, 00-4300-54). Single-cell suspensions derived from tumors were blocked with rat anti-mouse FcγIII/II receptor (CD16/CD32) blocking antibodies (“Fc-Block,” BioLegend, 156604) and stained with live/dead cell-exclusion dye (Zombie Yellow dye; BioLegend, 77168). The cells were then incubated for 30 minutes with fluorophore-conjugated antibodies described in Supplementary Table S3. Cells were subsequently washed, resuspended in FACS buffer, and analyzed using the Novocyte Quanteon flow cytometry system (Agilent). For granzyme B staining, cells were fixed and permeabilized with the Foxp3/Transcription Factor Staining Buffer Set (eBioscience, 00-5523-20) after surface staining. Flow cytometry analyses of cell populations were performed using FlowJo software version 10.8.1.

### Patient samples

Archived frozen pretreatment metastatic melanoma tissue samples were obtained through the Tissue Bank at Herbert Irving Comprehensive Cancer Center (HICCC). The Histology Service at HICCC performed sectioning and histopathologic interpretation. Frozen sections were used for immunostaining.

### Identification of T-cell exclusion program signature genes and correlational analysis with ANGPT2 expression in human melanoma

To generate the exclusion program in malignant cells associated with CD8<sup>+</sup> T-cell abundance, we utilized a single-cell RNA-sequencing (RNA-seq) dataset of 33 human melanoma tumors (GSE115978) applying the analytic codes provided from a previous study (37) and specified GitHub repository (<https://github.com/livnatje/ImmuneResistance>). To define an exclusion program signature gene, we followed the same procedures described in the previous study (37). First, to identify a cell-type specific gene for malignant cells and CD8<sup>+</sup> T cells, we used eight different cell subsets distinguished by gene expression and copy-number variation profiles. By calculating pairwise comparisons between the cell types via Wilcoxon rank sum-test, we obtained the

genes enriched for malignant cells ( $n = 389$ ) and CD8<sup>+</sup> T cells ( $n = 50$ ). Then, we computed the overall expression (OE) of the CD8<sup>+</sup> T-cell-specific genes in 474 Skin Cutaneous Melanoma (SKCM) from The Cancer Genome Atlas (TCGA) RNA-seq V2 expression dataset (obtained from <https://xenabrowser.net/datapages/>) to estimate CD8<sup>+</sup> T-cell abundance. The bulk RNA-seq data are an RSEM normalized count with log<sub>2</sub> transformation. We prioritized a seed exclusion gene based on a Pearson correlation between the expression of malignant cell-specific genes and the OE of the CD8<sup>+</sup> T-cell-specific genes. We selected 20 malignant genes as seed exclusion-up signature genes showing the most significant negative correlation with CD8<sup>+</sup> T-cell abundance, and 20 seed exclusion-down signature genes with the most significant positive correlation. We then calculated the correlation between the OE of seed exclusion genes and individual genes using a partial Spearman correlation and prioritized them by coefficient ranks. An exclusion signature gene is defined as the following: (i) exclusion-up: genes showing a significant positive correlation with seed exclusion-up signature and a negative correlation with seed exclusion-down signature; and (ii) exclusion-down: genes showing a significant positive correlation with seed exclusion-down signature and a negative correlation with seed exclusion-up signature. To compare the association between T-cell exclusion signatures and ANGPT2 expression, we stratified the TCGA-SKCM samples into three groups according to the expression profile of ANGPT2: (i) high expression ( $n = 48$ , >90th percentile), (ii) moderate expression ( $n = 189$ , 50th to 90th percentile), and (iii) low expression ( $n = 237$ , <50th percentile). For this, we converted the log<sub>2</sub> expression of each gene into a standardized z-score across samples and calculated the average of an exclusion signature gene for individual tumor samples. We compared the z-scores of the exclusion signature groups by ANGPT2 expression groups.

### Morphometric measurements

Images of whole tumor cross-sections and representative regions were taken using Axio Observer 7 with Apotome2 [Zeiss, 10× (N.A. 0.45) or 20× (N.A. 0.8) objective, bin 1 or 2], and image analysis was performed using MATLAB and ImageJ software. After defining the tumor region, we used the bwdist function in MATLAB and calculated distance from tumor margin. Immune cell infiltration was separately measured as CD8<sup>+</sup> T-cell count per mm<sup>2</sup> in the tumor periphery (<500 μm from tumor boundary) or tumor core (>500 μm from tumor boundary). Tumor proliferation and apoptosis were measured as the area of Ki-67 or cleaved-activated caspase-3-positive immunoreactivity, respectively, divided by total measured tumor area and presented as percentages. Necrosis was identified by the absence of DAPI staining of nuclei and was calculated as a percentage of the total tumor area. The ANGPT2/TIE2 pathway (ANGPT2, TIE2, p-TIE2, FOXO1), vascular leakage [fibrinogen], and vascular stability (desmin, VE-cadherin, claudin-5, type IV collagen) were measured as positive vascular area divided by total CD31<sup>+</sup> or VE-cadherin<sup>+</sup> blood vessel area and presented as percentages. Vascular density was measured as CD31<sup>+</sup> or VE-cadherin<sup>+</sup> vessel area divided by the total measured tumor area and presented as a percentage. Whole tumor cross-sections were imaged and analyzed for CD31, CD8, and Ki-67. One to three representative regions of the tumor periphery and core were imaged and analyzed for remaining readouts, except for cleaved-activated caspase-3, for which, only representative images of the tumor core were imaged and quantified.

### RT-qPCR

Harvested tumor tissues were dipped into liquid nitrogen to extract total RNA using RNeasy Mini Kit (Qiagen, 74134) and tissue

homogenizing tubes with beads (Thermo Fisher Scientific, 15-340-153). Total 1 µg of RNA was reverse transcribed into cDNA using the qScript cDNA Synthesis Kit (Quantabio, 95048-100). Gene expression was quantified with PerfeCTa SYBR Green FastMix (Quantabio, 95074-012) and QuantStudio 5 Real-Time PCR System (Applied Biosystems). GAPDH was used as an internal reference gene. Primer sequences are listed in Supplementary Table S4.

### Statistical analysis

Data are presented as mean SEM. *P* values indicating statistical significance are presented in figures (*P* ≥ 0.05 not labeled). Differences between the means of regions within the same sample were compared by paired two-tailed Student *t* test. Statistical differences between the means of two different groups were compared by unpaired two-tailed Student *t* test, unless otherwise noted. For tumor growth curves of two groups, statistical significance between average tumor volumes was evaluated at the final presented time point by Mann–Whitney test. Statistical differences between multiple groups, including average tumor volumes at the final presented time point, were compared by one-way ANOVA with Tukey correction for multiple comparisons. Statistical analyses were performed using GraphPad Prism version 9.1.0. For analysis of single-cell RNA-seq, statistical evaluation was conducted by pairwise Wilcoxon rank-sum test.

### Data availability

All data accessed from external sources and prior publications have been referenced in the article and Supplementary Data files. The single-cell RNA-seq data analyzed in this study (GSE115978) were obtained from Gene Expression Omnibus (GEO). The bulk RNA-seq data from the TCGA SKCM cohort analyzed in this study were obtained from the TCGA RNA-seq V2 expression dataset at <http://xenabrowser.net/datapages/>. All other raw data are available upon request from the corresponding author.

## Results

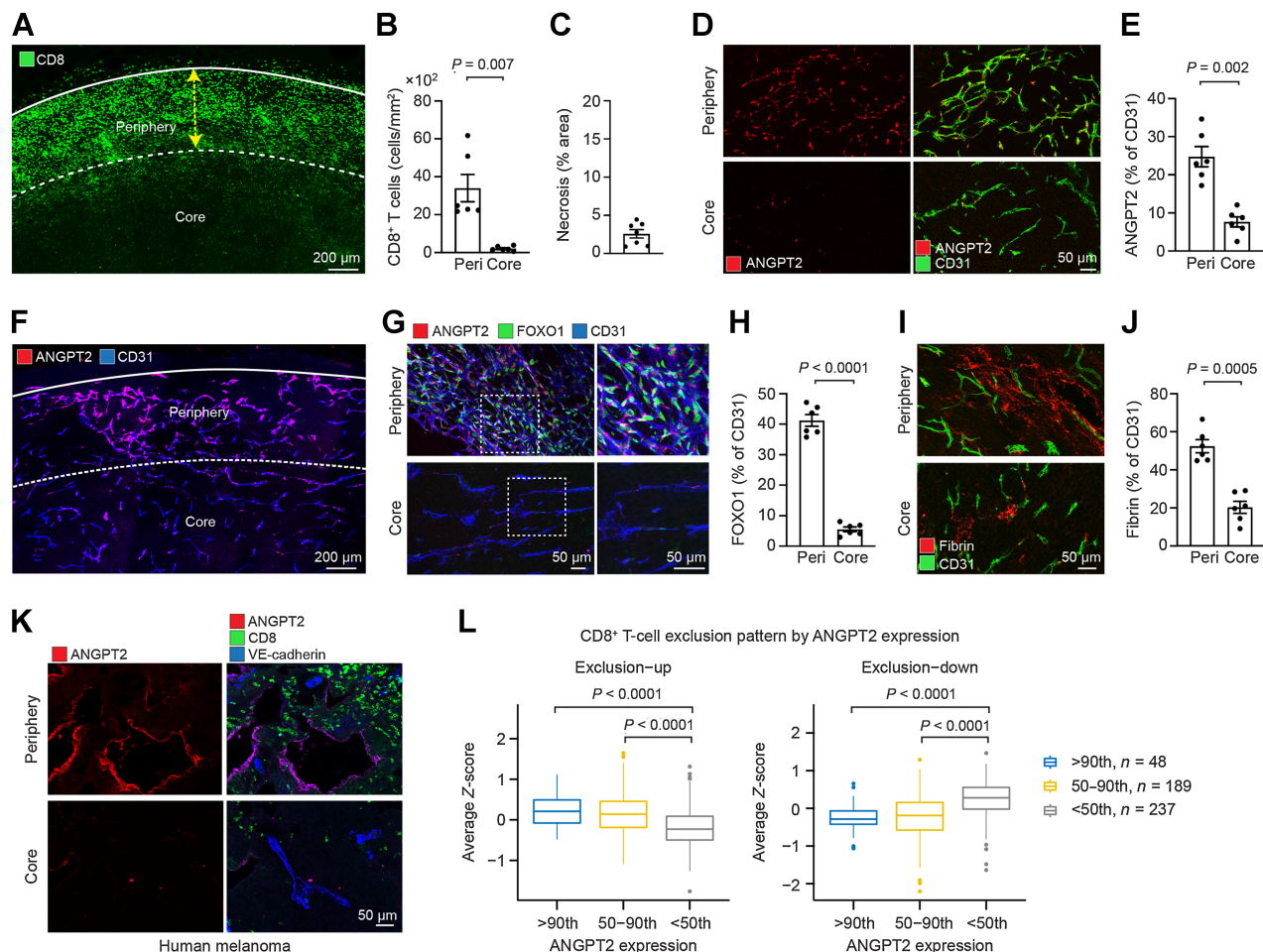
### T-cell exclusion is associated with spatial ANGPT2 upregulation and vascular destabilization at the tumor periphery

We sought to understand CD8<sup>+</sup> T-cell distribution in genetically defined syngeneic melanoma models of YUMM1.7 (35) and YUMMER1.7 (*Braf*<sup>V600E</sup>, *Pten*<sup>-/-</sup>, and *Cdkn2a*<sup>-/-</sup>; ref. 34) as well as B16-F10 melanoma, each characterized by different levels of tumor immunogenicity. Unlike the parental YUMM1.7 tumor model, YUMMER1.7 melanoma cells have been irradiated with ultraviolet B radiation and thus harbor additional somatic mutations, generating an immunogenic TME. Notably, subcutaneous YUMMER1.7 tumors recapitulated the clinically important phenotype of impaired T-cell infiltration into the tumor core, characterized by a large proportion of CD8<sup>+</sup> T cells retained in the tumor periphery (<500 µm from the tumor margin) and blocked from the core (“T-cell exclusion”; Fig. 1A and B). On average, only 2.5% of total tumor area was necrotic, primarily limited to the tumor core (Fig. 1C). Similar to YUMMER1.7, the less immunogenic YUMM1.7 tumors exhibited T-cell exclusion from the core, despite lower overall CD8<sup>+</sup> T-cell density. B16-F10 tumors also showed CD8<sup>+</sup> T-cell restriction to the tumor periphery, displaying the lowest population of CD8<sup>+</sup> T cells among the melanoma mouse models we examined (Supplementary Fig. S1).

To understand the spatial association of ANGPT2/TIE2 signaling with T-cell exclusion in melanoma, we first evaluated ANGPT2, total TIE2, and phosphorylated TIE2 (p-TIE2) expression in murine mel-

anomas. To directly compare ANGPT2/TIE2 signaling in tumor and adjacent normal tissues, we studied pulmonary metastases and surrounding healthy tissues 3 weeks after intravenous tumor cell inoculation of YUMMER1.7 and B16-F10. By performing immunostaining with an anti-ANGPT2 antibody (REGN910; ref. 38), we found significantly elevated levels of endothelial ANGPT2 accompanied by reductions in p-TIE2 and total TIE2 levels in pulmonary metastatic lesions (Supplementary Fig. S2A–S2C). In contrast, vessels in the adjacent healthy lungs showed weak or no ANGPT2 expression and high p-TIE2 and TIE2 levels. When we compared ANGPT2 expression in tumors collected 4 weeks after subcutaneous YUMMER1.7 cell inoculation, vessels in the tumor periphery had higher ANGPT2 expression than those in the tumor core (Fig. 1D and E). Consistently, whole tumor cross-sections of YUMMER1.7 melanoma showed high endothelial ANGPT2 expression at the tumor periphery (Fig. 1F). Using single-cell RNA-seq datasets of human melanoma (37), we also analyzed ANGPT2 expression in different cell types. Although the cellular expression profile showed the highest expression of ANGPT2 in endothelial cells, ANGPT2 was also detectable in other cell types such as malignant cells (Supplementary Fig. S3A and S3B). To understand the link between TIE2 activity and ANGPT2 expression, we explored the activity of FOXO1 in blood vessels of the tumor periphery and core. Previous evidence showed that TIE2 signaling activation promotes downstream PI3K/Akt signaling and consequently results in FOXO1 phosphorylation, leading to nuclear exclusion, ubiquitination, and degradation of FOXO1, whereas TIE2/PI3K/Akt signaling suppression induces nuclear accumulation and activation of FOXO1 (19, 20). We found strong nuclear FOXO1 in tumor blood vessels at the periphery where ANGPT2 expression was high but little to no nuclear FOXO1 or ANGPT2 in endothelial cells of the tumor core (Fig. 1G and H). These findings align with evidence that elevated ANGPT2 expression is a consequence of FOXO1 transcriptional activation resulting from TIE2 signaling suppression (39, 40). Functionally, elevated endothelial ANGPT2 in the tumor periphery spatially coincided with greater vascular leakage evidenced by extravasated plasma stained with fibrin(ogen) outside of tumor vessels (Fig. 1I and J). Our data support that endothelial ANGPT2 upregulation and increased vascular leakage are spatially associated with T-cell accumulation in the periphery of tumor nests.

Human melanoma metastatic tissues consistently showed strong ANGPT2 expression in peripheral tumor blood vessels (<500 µm from the tumor margin) concomitant with CD8<sup>+</sup> T-cell abundance, contrasting regions of the tumor core showing weak endothelial ANGPT2 expression with limited CD8<sup>+</sup> T-cell infiltration (Fig. 1K). To further delineate the relationship between ANGPT2 expression and T-cell exclusion, we examined the genes strongly correlated with T-cell exclusion in melanoma using single-cell and bulk RNA-seq datasets (37). We identified cell-type specific genes for malignant cells and CD8<sup>+</sup> T cells and inferred T-cell infiltration levels in tumors from the 474 bulk RNA-seq profiles of TCGA-SKCM (41). Then, we defined 225 “exclusion-up” genes that were negatively correlated with T-cell infiltration and were induced in non-inflamed or cold tumors, and 162 “exclusion-down” genes that were positively correlated with T-cell infiltration. The induced part of the program (exclusion-up) was enriched for genes involved in transcriptional and translational regulation (e.g., *SOX4* and *EIF3H*), whereas the repressed part of the program (exclusion-down) included genes involved in apoptosis (e.g., *PERP* and *IFI27L2*) and immune modulation (e.g., *IRF4*; Supplementary Fig. S4). Next, we evaluated whether ANGPT2 is associated with the exclusion program signature genes in human melanoma. From the

**Figure 1.**

Endothelial ANGPT2 upregulation and increased vascular leakage are spatially associated with T-cell accumulation in the tumor periphery. For these studies,  $2.5 \times 10^5$  YUMMER1.7 (*Braf*<sup>V600E</sup>, *Pten*<sup>-/-</sup>, and *Cdkn2a*<sup>-/-</sup>) cells were subcutaneously inoculated in C57BL/6 mice. Tumors were collected 4 weeks after cell inoculation. **A** and **B**, Representative images showing accumulation of CD8<sup>+</sup> T cells in the tumor periphery (<500 μm from tumor margin; top) and sparse CD8<sup>+</sup> T-cell distribution in the tumor core (**A**) and corresponding quantification of CD8<sup>+</sup> T cells ( $n = 6$ ; **B**). **C**, Proportion of necrosis identified by the absence of DAPI staining of nuclei in the entire tumor ( $n = 7$ ). **D** and **E**, Images comparing ANGPT2 expression (red) in tumor vessels (CD31; green) in the tumor periphery (<500 μm from tumor margin; top) and core (bottom; **D**) and corresponding quantification showing higher ANGPT2 expression in the tumor periphery ( $n = 6$ ; **E**). **F**, Representative image showing strong endothelial ANGPT2 immunoreactivity (red) in the tumor periphery. Solid line represents the tumor boundary and dotted line represents the boundary between tumor periphery and core. **G** and **H**, Representative images showing strong nuclear FOXO1 (green) and cytoplasmic ANGPT2 (red) expression in blood vessels (CD31; blue) of the tumor periphery unlike weak or absent FOXO1 and ANGPT2 expression in vessels of the tumor core (**G**) and corresponding quantification ( $n = 6$ ; **H**). **I** and **J**, Representative images comparing tumor vascular leakage shown by extravasated fibrinogen (red) in the tumor periphery (top) and core (bottom; **I**) and corresponding quantification showing greater vascular leakage in the tumor periphery ( $n = 6$ ; **J**). For **B**, **C**, **E**, **H**, and **J**, each data point represents individual mouse. Data combine two independent experiments. Error bars, SEM. *P* values as shown. Statistical analysis by paired two-tailed Student *t* test. **K**, Representative images of pretreatment human melanoma brain metastasis showing accumulation of CD8<sup>+</sup> T cells (green) and corresponding high ANGPT2 expression (red) in the tumor periphery (<500 μm from tumor margin; top) compared with low CD8<sup>+</sup> T-cell infiltration and weak endothelial ANGPT2 expression in the tumor core (bottom). **L**, Gene expression pattern of T-cell exclusion program (exclusion-up, left; exclusion-down, right) in human melanomas with differential ANGPT2 expression (TCGA-SKKCM data set, >90th,  $n = 48$ ; 50–90th,  $n = 189$ ; <50th,  $n = 237$  expression percentile). *P* values as shown ( $P \geq 0.05$  not labeled). Statistical analysis by pairwise Wilcoxon rank-sum test.

TCGA-SKKCM bulk RNA-seq data, we categorized tumor samples into three groups divided by ANGPT2 expression levels and found a strong correlation between ANGPT2 expression and CD8<sup>+</sup> T-cell exclusion signatures. The ANGPT2 high group (>90th percentile) exhibited a significantly higher expression of exclusion-up signature genes than the ANGPT2 low group (<50th;  $P < 0.0001$ ; Fig. 1L). In contrast, exclusion-down genes have significantly higher expression in the ANGPT2 low group compared with the ANGPT2 high group ( $P < 0.0001$ ). Together, these results suggest that the spatial ANGPT2

upregulation and elevated vascular leakage in the tumor periphery could be involved in T-cell exclusion.

#### Pharmacologic inhibition and genetic deletion of ANGPT2 reduce T-cell exclusion

To investigate ANGPT2 regulation of T-cell exclusion, we tested whether ANGPT2 neutralization using selective anti-ANGPT2 antibody (REGN910; ref. 38) promotes T-cell infiltration into the tumor core in YUMMER1.7 and YUMM1.7 mouse melanomas (Fig. 2A).

Importantly, although control YUMMER1.7 tumors showed preferential CD8<sup>+</sup> T-cell localization to the tumor periphery, pharmacologic ANGPT2 inhibition increased the number of CD8<sup>+</sup> T cells to the tumor core (**Fig. 2B** and **C**). Specifically, ANGPT2 blockade increased the number of CD8<sup>+</sup> T cells by 91% in the core. We also observed that T-cell density was frequently variable within the tumor cores following ANGPT2 inhibition, independent of tumor necrosis (Supplementary Fig. S5A and S5B). Analysis of CD8<sup>+</sup> T-cell abundance in whole tumor cross-sections showed that ANGPT2 inhibition reduced the spatial discrepancy in T-cell density between the tumor periphery and core by increasing T-cell infiltration to the core (**Fig. 2D** and **E**). Furthermore, in the less immunogenic YUMM1.7 tumor model, ANGPT2 inhibition showed a 75% increase of CD8<sup>+</sup> T-cell infiltration in the tumor core (**Fig. 2F** and **G**). To further delineate whether the genetic targeting of ANGPT2 improves CD8<sup>+</sup> T-cell infiltration to the tumor center, we investigated CD8<sup>+</sup> T-cell distribution in the tumors of *Angpt2*<sup>iΔEC</sup> mice, which are generated by crossing *Angpt2*<sup>fl/fl</sup> mice (31, 32) with VE-cadherin-Cre-ER<sup>T2</sup> mice (33), after YUMMER1.7 inoculation (**Fig. 2H**). We first confirmed low or absent ANGPT2 expression on blood vessels at the tumor periphery and core of *Angpt2*<sup>iΔEC</sup> mice (Supplementary Fig. S6A and S6B). Consistently, we observed significantly improved CD8<sup>+</sup> T-cell infiltration in the tumor cores of *Angpt2*<sup>iΔEC</sup> mice, compared with age-matched wild-type controls exhibiting the expected pattern of CD8<sup>+</sup> T-cell exclusion (**Fig. 2I** and **J**). Tumors from *Angpt2*<sup>iΔEC</sup> mice exhibited a 98% increase in CD8<sup>+</sup> T cells in the tumor core, closely resembling the observed patterns in YUMMER1.7 tumors pharmacologically targeted for ANGPT2.

Analysis of flow cytometry following dissection of the tumor periphery and core also showed a higher frequency of CD8<sup>+</sup> T cells at the tumor periphery compared with the core of control YUMMER1.7 tumors, with similar patterns observed for CD45<sup>+</sup> cells and CD4<sup>+</sup> T cells (Supplementary Fig. S7A–S7C). Inhibition of ANGPT2 reduced the spatial discrepancy in CD45<sup>+</sup> and CD8<sup>+</sup> T-cell frequencies between the tumor periphery and core by increasing the proportion of these cells in the tumor core. Although ANGPT2 blockade did not affect the frequency of total CD4<sup>+</sup> T cells in the tumor core, it reduced the frequency of CD4<sup>+</sup> T cells in the tumor periphery. Furthermore, we found that ANGPT2 inhibition decreased the proportion of regulatory T cells (Tregs: CD4<sup>+</sup>Foxp3<sup>+</sup>) in the tumor core (Supplementary Fig. S7D). Unlike for T cells, the exclusion pattern was less evident for tumor-associated macrophages (TAM), TEMs, and mononuclear or polymorphonuclear myeloid-derived suppressor cells (M-MDSC or PMN-MDSC) in control YUMMER1.7 tumors (Supplementary Fig. S7E–S7I). There were also no significant changes observed in the frequencies of TAM, TEMs, and M-MDSCs in tumors following ANGPT2 inhibition, which only increased the PMN-MDSCs in the tumor core. However, we found that ANGPT2 blockade increased M1/M2 ratio (M1-like TAMs: CD206<sup>low</sup>CD11c<sup>high</sup> and M2-like TAMs: CD206<sup>high</sup>CD11c<sup>low</sup>) in both tumor periphery and core due to increased frequencies of M1-like TAMs involved in proinflammatory responses (42). Taken together, our data demonstrate that targeting ANGPT2 promotes CD8<sup>+</sup> T-cell infiltration into the tumor core, highlighting ANGPT2 as a key regulator of CD8<sup>+</sup> T-cell exclusion in the tumors.

#### ANGPT2 inhibition restores TIE2 signaling and stabilizes vessels of the tumor periphery

To test our hypothesis that tumor vascular destabilization, resulting from ANGPT2-mediated TIE2 signaling suppression, serves as a barrier impairing effective T-cell infiltration to the tumor core, we

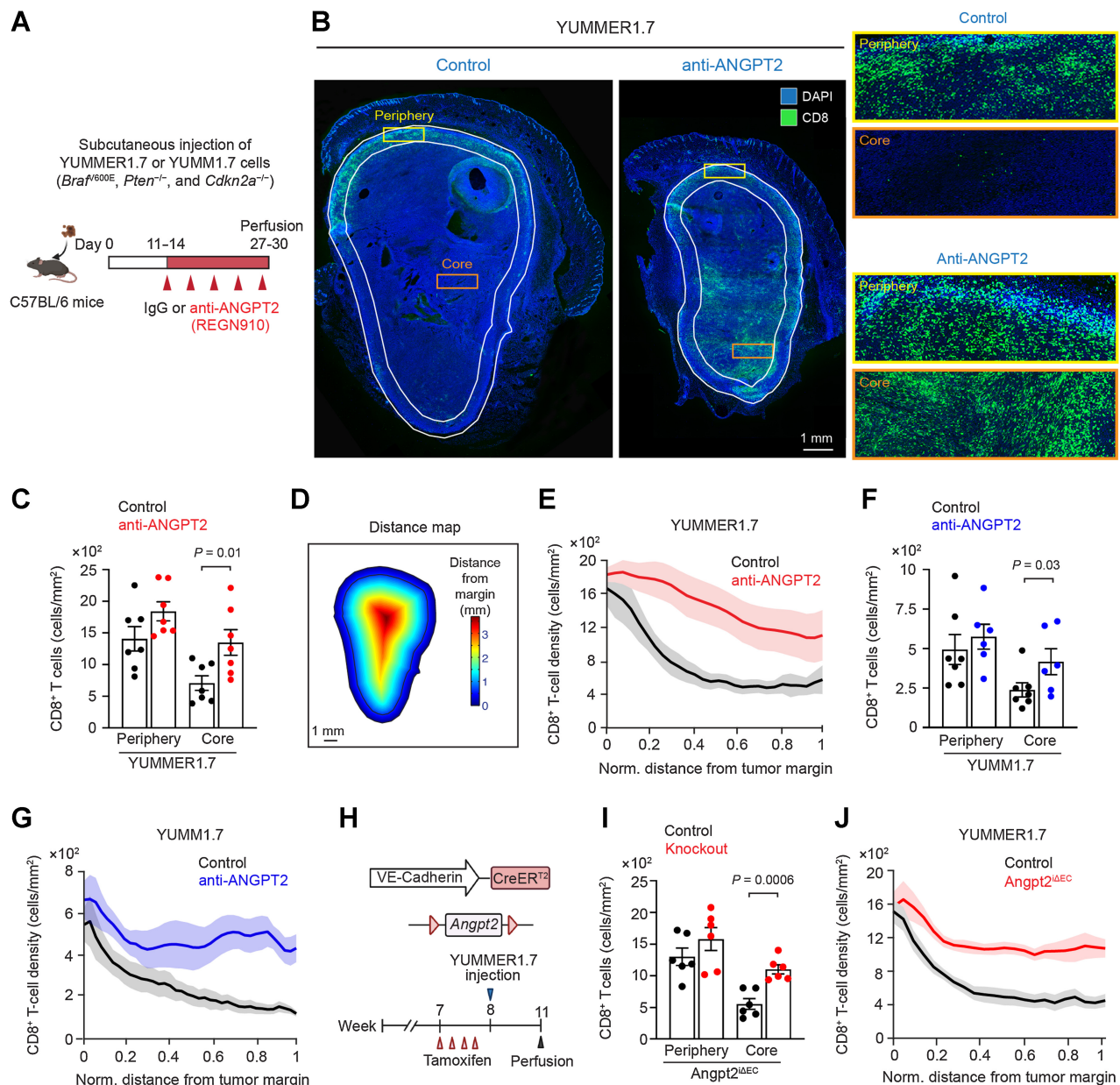
investigated the effects of ANGPT2 inhibition on TIE2 activity and vascular integrity at the tumor periphery and core, respectively. We found that tumor vessels at both the periphery and core of YUMMER1.7 tumors showed significant suppression of TIE2 signaling, evidenced by low TIE2 and p-TIE2 immunoreactivities in endothelial cells of control tumors, contrasting adjacent healthy vessels in the skin showing high p-Tie2 levels (**Fig. 3A–D**; Supplementary Fig. S8). ANGPT2 inhibition by REGN910 treatment significantly increased TIE2 expression (3.9- and 3.7-fold in the periphery and core, respectively), which primarily showed a concentrated distribution in the cytoplasm (**Fig. 3A** and **B**). It is noteworthy that ANGPT2 blockade increased p-TIE2 levels, with a more prominent effect in blood vessels of the tumor periphery (8.8-fold) compared with vessels of the tumor core (2.4-fold; **Fig. 3C** and **D**).

In our analyses of structural and functional changes of blood vessels in the tumor periphery and core, targeting ANGPT2 increased desmin<sup>+</sup> pericyte coverage (2.7- and 1.9-fold in periphery and core, respectively), distribution of the endothelial junctional molecules VE-cadherin (4.8- and 2.3-fold in the periphery and core, respectively) and claudin-5 (2.8- and 1.5-fold in the periphery and core, respectively), and type IV collagen<sup>+</sup> basement membrane coverage (1.2-fold for both periphery and core) on tumor vessels (**Fig. 3E**; Supplementary Fig. S9). Consistent with previous studies (38, 43), the pharmacologic blockade of ANGPT2 decreased tumor vascular density in the whole tumor (**Fig. 3F** and **G**) in addition to exerting significant vascular stabilization. Importantly, we observed that ANGPT2 inhibition reduced vascular leakage measured by fibrin(ogen) by 61% in blood vessels in the tumor periphery and by 20% in tumor core (**Fig. 3H** and **I**).

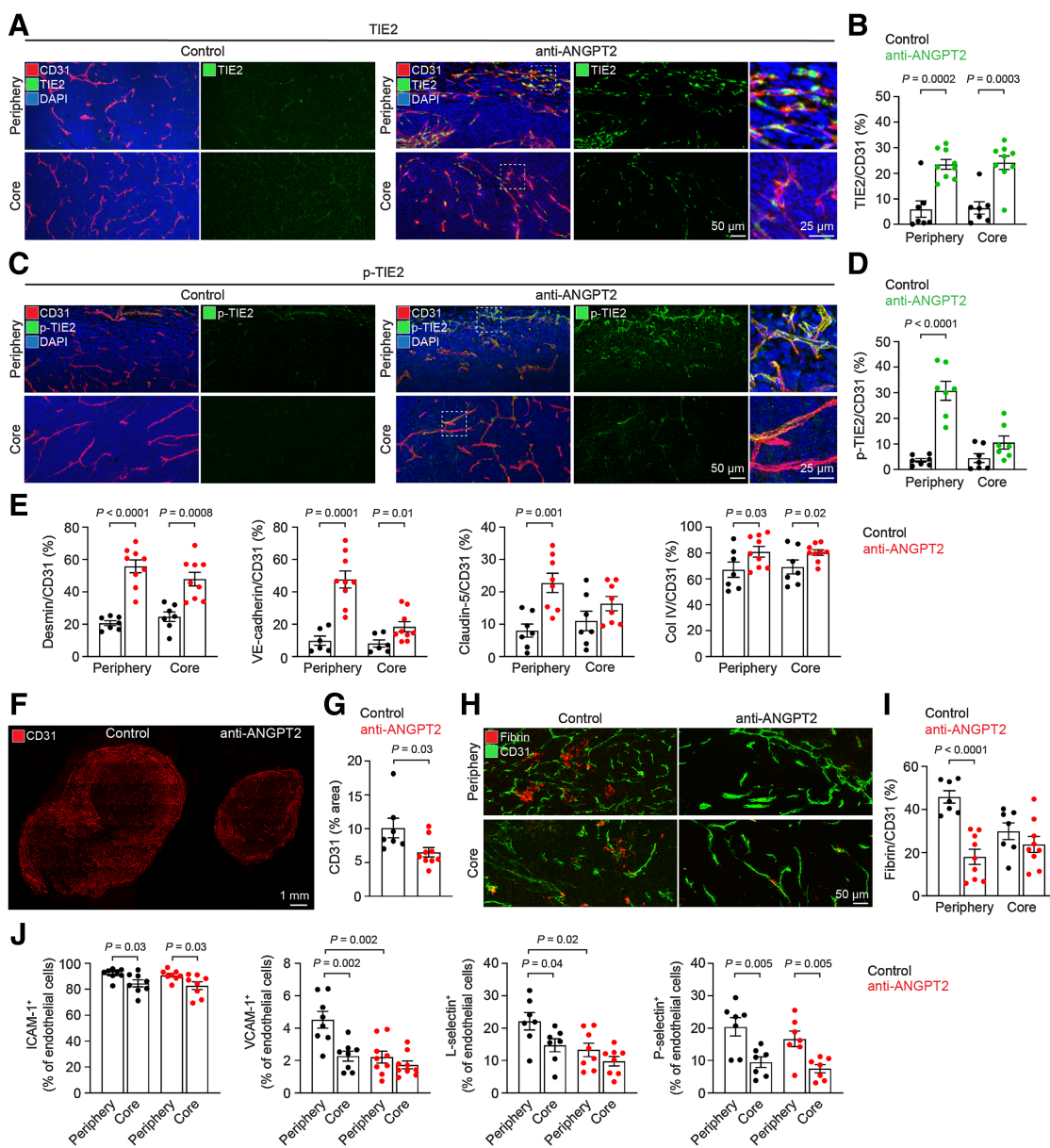
To identify a mechanism by which vascular changes following ANGPT2 inhibition reduce T-cell exclusion, we investigated the expression patterns of adhesion molecules on endothelial cells in the tumor periphery and core, respectively. We found that endothelial cell expression of adhesion molecules, including vascular cell adhesion molecule 1 (VCAM-1), was higher in the tumor periphery than in the core of control YUMMER1.7 tumors (**Fig. 3J**). Interestingly, treatment with anti-ANGPT2 reduced the frequency of endothelial cells expressing adhesion molecules, especially VCAM-1 and L-selectin, in the tumor periphery, thereby decreasing spatial discrepancies in adhesion molecule expression between the tumor periphery and core. Furthermore, we tested for disrupted chemokine gradients between the periphery and core of control tumors, which can lead to an exclusion phenotype. However, we found similar expression levels in CXCL9, CXCL10, and CXCL11, which are responsible for T-cell recruitment, between the periphery and core of control tumors (Supplementary Fig. S10). Not only does our data support previous findings that antiangiogenic therapy enhances vascular integrity, but our findings indicate that ANGPT2 inhibition preferentially promotes TIE2 signaling activation and the reversal of vascular destabilization at the tumor periphery, where the expression of endothelial cell adhesion molecules is also reduced.

#### Targeting ANGPT2 reduces tumor growth in mouse melanomas of differing tumor immunogenicity

Given the reversal of T-cell exclusion together with improved vascular integrity at the tumor periphery following ANGPT2 inhibition, we next evaluated the antitumor effects of targeting ANGPT2 in YUMMER1.7 and YUMM1.7 melanomas after treatment with human IgG or anti-ANGPT2 antibody for 2 weeks. Pharmacologic ANGPT2 inhibition significantly reduced the rate of YUMMER1.7 tumor growth compared with IgG-treated controls ( $P = 0.0004$ ; **Fig. 4A**). Consistent with delayed tumor growth following ANGPT2 blockade,

**Figure 2.**

Pharmacologic inhibition and genetic deletion of ANGPT2 promote CD8<sup>+</sup> T-cell infiltration to the tumor core. YUMMER1.7 ( $2.5 \times 10^5$ ) or YUMM1.7 ( $5 \times 10^5$ ) cells were subcutaneously inoculated in C57BL/6 or *Angpt2*<sup>ΔEC</sup> mice. **A**, C57BL/6 mice were administered anti-ANGPT2 (REGN910, 12.5 mg/kg i.p.) or human IgG (REGN1945, 12.5 mg/kg i.p.) when tumors were  $\sim 70$  mm<sup>3</sup> in volume for five total doses. **B**, Representative images comparing CD8<sup>+</sup> T-cell (green) abundance in whole tumor cross-sections (left) and in magnified regions of the tumor periphery and core (right) from YUMMER1.7 mice treated with IgG or anti-ANGPT2. **C**, Corresponding quantification of CD8<sup>+</sup> T-cell count per mm<sup>2</sup> showing elevated infiltration in YUMMER1.7 tumors after ANGPT2 blockade (IgG,  $n = 7$ ; anti-ANGPT2,  $n = 7$ ). **D**, Distance map showing method for analyzing CD8<sup>+</sup> T-cell count as a function of distance from the tumor margin, applied to generate **E**, **G**, and **J**. **E**, CD8<sup>+</sup> T-cell density graphs reflect a growing difference in CD8<sup>+</sup> T-cell density between control and experimental groups with increased distance from the tumor margin. For **C**, **F**, and **I**, each data point represents individual mouse. Error bars, SEM. *P* values as shown ( $P \geq 0.05$  not labeled). Statistical analysis by unpaired two-tailed or one-tailed Student *t* tests. **H**, Diagram depicting the generation of *Angpt2*<sup>ΔEC</sup> mice and experimental schedule consisting of four consecutive tamoxifen injections prior to cell inoculation. Tumors were collected 4 weeks after YUMMER1.7 cell inoculation.

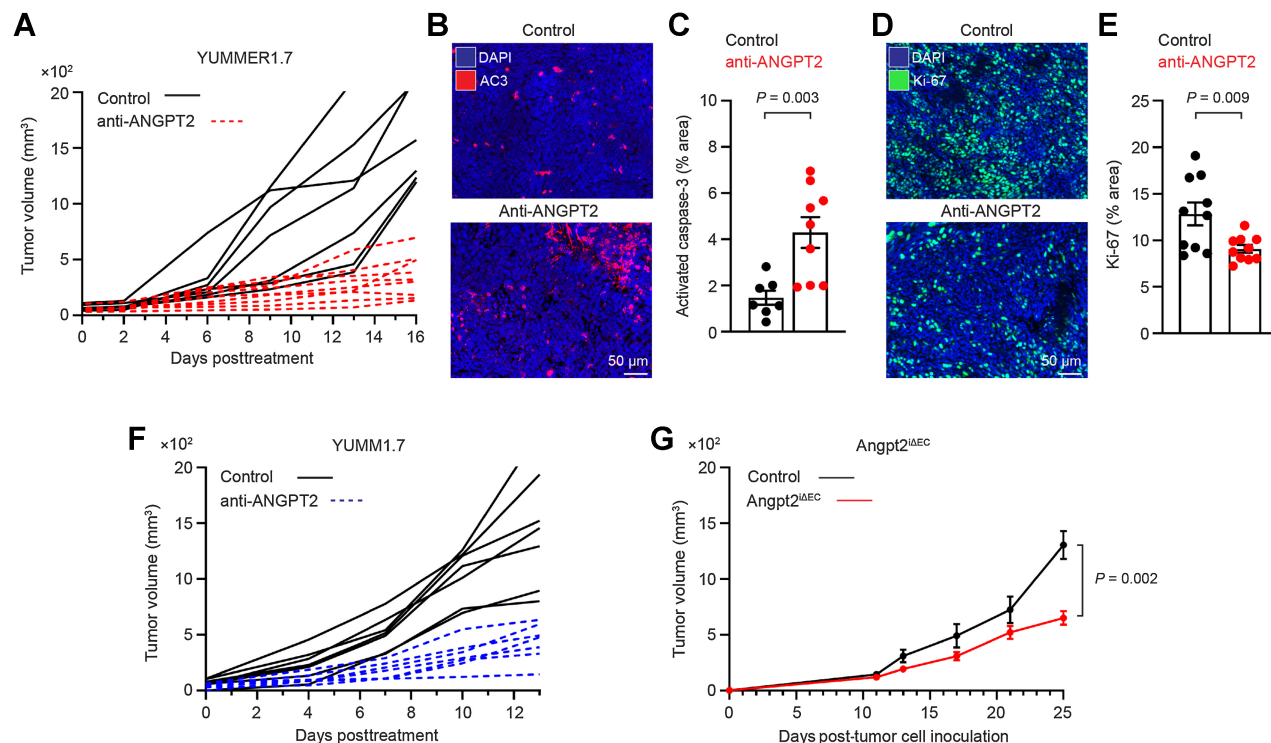
**Figure 3.**

ANGPT2 inhibition restores TIE2 activity and improves vascular integrity in YUMMER1.7 tumors. C57BL/6 mice subcutaneously inoculated with YUMMER1.7 cells were treated with anti-ANGPT2 or human IgG as shown in Fig. 2A. **A** and **B**, Representative images of TIE2 expression (green) on tumor vessels (CD31; red) in the periphery (top) and core (bottom) of IgG (left) and anti-ANGPT2 (right)-treated tumors (**A**) and corresponding quantification (**B**) showing significant elevation in TIE2 expression, measured as a percent area of CD31<sup>+</sup> tumor blood vessels, after ANGPT2 blockade compared with IgG controls (IgG,  $n = 7$ ; anti-ANGPT2,  $n = 9$ ). **C** and **D**, Comparison of phosphorylated TIE2 (p-TIE2; green) in the tumor periphery (top) and core (bottom) after IgG (left) and anti-ANGPT2 (right) treatment (**C**) and corresponding quantification (**D**) showing increased p-TIE2 levels after ANGPT2 blockade (IgG,  $n = 7$ ; anti-ANGPT2,  $n = 7$ ). For **B** and **D**, statistical analysis by unpaired two-tailed Student *t* test. **E**, Quantifications comparing desmin<sup>+</sup> pericyte coverage, VE-cadherin<sup>+</sup> and claudin-5<sup>+</sup> endothelial junctions, and type IV collagen<sup>+</sup> basement membrane coverage at the tumor periphery and core after IgG ( $n = 6$ –7) or anti-ANGPT2 ( $n = 8$ –9) treatment. Data combine three independent experiments. Statistical analysis by unpaired two-tailed or one-tailed Student *t* test. **F** and **G**, Representative images of whole-tumor sections comparing vascular density (CD31; red) after IgG or anti-ANGPT2 treatment (**F**) and corresponding quantification (**G**) showing significant reduction in vascular density after anti-ANGPT2 therapy compared with IgG (IgG,  $n = 7$ ; anti-ANGPT2,  $n = 9$ ). **H**, Representative images of tumor vascular leakage measured by extravasated fibrinogen (red) from tumor vessels (CD31; green) in the periphery and core after IgG and anti-ANGPT2 treatment. **I**, Quantification, measured as a percent area of CD31<sup>+</sup> tumor blood vessels, showing a significant reduction in extravasated fibrinogen in the tumor periphery after ANGPT2 blockade (IgG,  $n = 7$ ; anti-ANGPT2,  $n = 9$ ). Data combine three independent experiments. Statistical analysis by unpaired two-tailed Student *t* test. **J**, Flow cytometry analysis comparing expression of intercellular adhesion molecule 1 (ICAM-1), vascular cell adhesion molecule 1 (VCAM-1), L-selectin, and P-selectin on CD31<sup>+</sup> endothelial cells from the tumor periphery and core after IgG ( $n = 7$ –8) or anti-ANGPT2 ( $n = 7$ –8) treatment in YUMMER1.7 mice. Data combine two independent experiments. Statistical analysis by unpaired two-tailed Student *t* test. For **B**, **D**, **E**, **G**, **I**, and **J**, each data point represents individual mouse. Error bars, SEM. *P* values as shown ( $P \geq 0.05$  not labeled).

immunofluorescence staining analyses of cleaved-activated caspase-3 in tumors demonstrated that compared with IgG treatment, ANGPT2 inhibition promoted a significant rise in apoptosis (**Fig. 4B** and **C**). Furthermore, we found a reduction in cell proliferation after ANGPT2 inhibition in YUMMER1.7 melanoma (**Fig. 4D** and **E**). We confirmed consistently delayed tumor growth when treatments were extended until 4 weeks from treatment onset (Supplementary Fig. S11). In addition, YUMM1.7 tumors harboring lower immunogenicity also exhibited notably reduced rates of tumor growth after pharmacologic ANGPT2 inhibition ( $P = 0.0006$ ; **Fig. 4F**). To ascertain the impact of ANGPT2 on promoting the growth of melanoma, we investigated tumor growth after subcutaneous YUMMER1.7 cell inoculation in *Angpt2<sup>ΔEC</sup>* mice. Genetic deletion of endothelial ANGPT2 (*Angpt2<sup>ΔEC</sup>*) significantly delayed growth of YUMMER1.7 melanomas compared with tumor-bearing wild-type C57BL/6J controls (**Fig. 4G**). These data from mouse melanomas with the clinically relevant *Braf*, *Pten*, and *Cdkn2a* driver mutations support ANGPT2 as a potential therapeutic target to suppress the malignant growth of melanomas of differing tumor immunogenicity.

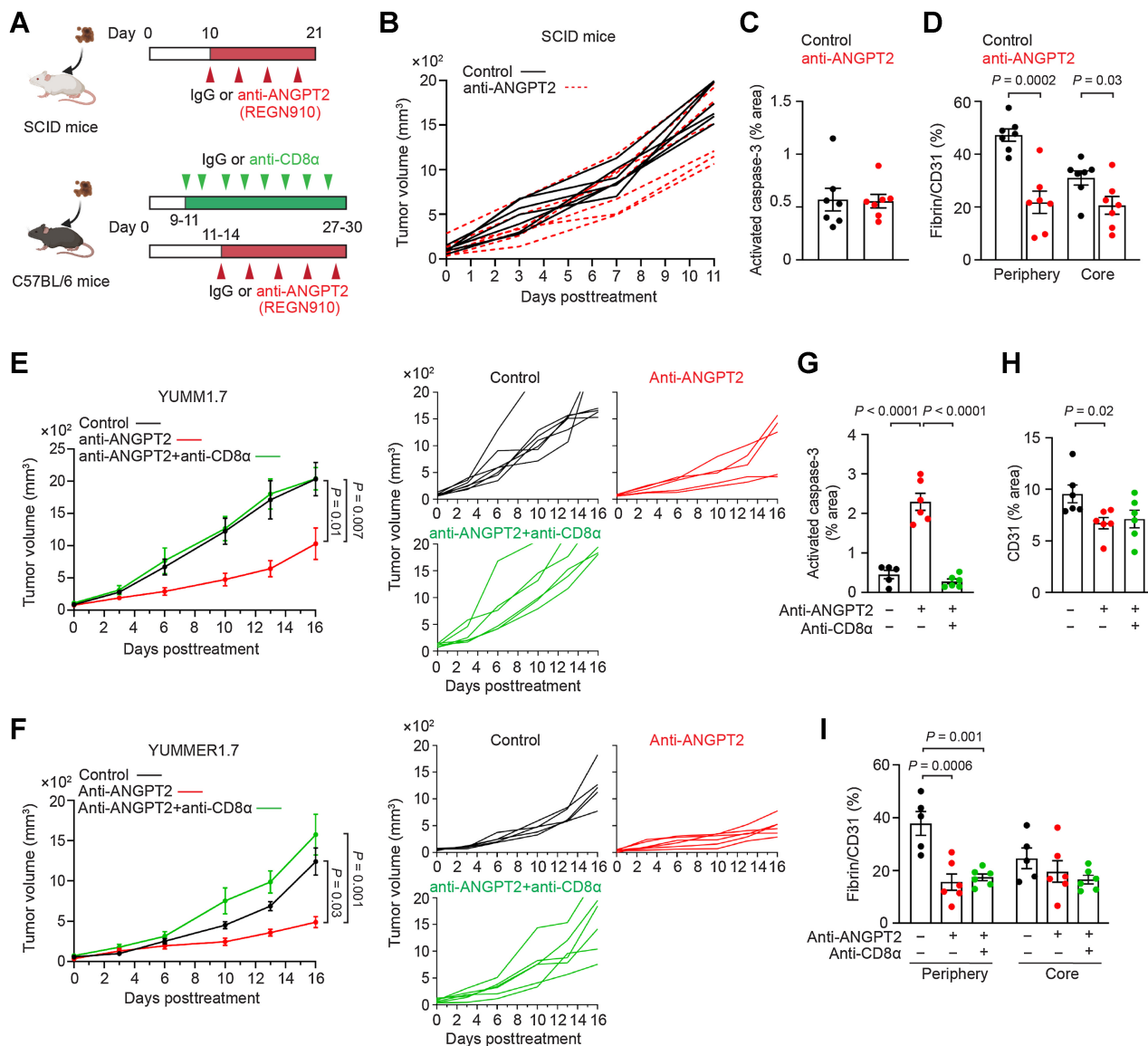
### Antitumor response mediated by ANGPT2 inhibition is dependent on CD8<sup>+</sup> T cells

To better understand the mechanism underlying the antitumor response driven by ANGPT2 inhibition, we inoculated immunodeficient mice lacking both T and B cells (SCID, C.B-*Igh-1<sup>b</sup>/IcrTac-Prkdc<sup>scid</sup>*) with YUMMER1.7 cells, investigating tumor growth after treatment with IgG or anti-ANGPT2 (**Fig. 5A**). We confirmed the absence of CD8<sup>+</sup> T cells in SCID mice through immunofluorescence staining of tumors (Supplementary Fig. S12A). Pharmacologic ANGPT2 inhibition did not delay tumor growth in SCID mice, showing comparable tumor burden and apoptosis between immunodeficient mice treated with IgG or REGN910 (**Fig. 5B** and **C**). Of note, despite no reduction in tumor burden, immunodeficient mice treated with REGN910 showed reduced vascular leakage and increased vascular VE-cadherin expression with greater differences in the tumor periphery compared with the core, consistent with our findings in immunocompetent mice (**Fig. 5D**; Supplementary Fig. S13). To ascertain the functional contribution of CD8<sup>+</sup> T cells to the therapeutic efficacy of ANGPT2 inhibition, we next depleted CD8<sup>+</sup> T cells in both YUMM1.7 and YUMMER1.7 mouse models



**Figure 4.**

Pharmacologic inhibition and genetic deletion of ANGPT2 slow tumor growth and increase apoptosis in mouse melanoma. C57BL/6 mice or *Angpt2<sup>ΔEC</sup>* mice subcutaneously inoculated with YUMMER1.7 or YUMM1.7 cells were treated with anti-ANGPT2 or human IgG as shown in **Fig. 2A** and **H**. **A**, Tumor growth of YUMMER1.7 (IgG,  $n = 7$ ; anti-ANGPT2,  $n = 9$ ) mice given ANGPT2 blockade (REGN910; dotted red line) or IgG (solid black line). **B** and **C**, Representative images of cleaved-activated caspase-3 (AC3; red) with DAPI (blue) in IgG (control; top)- and anti-ANGPT2 (bottom)-treated tumors (**B**) and corresponding quantification of AC3<sup>+</sup> percent area in the tumor core (**C**) showing increased apoptosis in anti-ANGPT2-treated YUMMER1.7 mice compared with IgG-treated controls (IgG,  $n = 7$ ; anti-ANGPT2,  $n = 9$ ). **D** and **E**, Representative images of Ki-67 (green) with DAPI (blue) in IgG (control; top)- and anti-ANGPT2 (bottom)-treated tumors (**D**) and corresponding quantification showing reduced tumor proliferation after ANGPT2 blockade in YUMMER1.7 mice (IgG,  $n = 10$ ; anti-ANGPT2,  $n = 10$ ; **E**). For **C** and **E**, each data point represents individual mouse. Error bars, SEM.  $P$  values as shown. Statistical analysis by unpaired two-tailed Student *t* test. **F**, Tumor growth of YUMM1.7 (IgG,  $n = 7$ ; anti-ANGPT2,  $n = 7$ ) mice given ANGPT2 blockade (REGN910; dotted blue line) or IgG (solid black line). For **A** and **F**, each curve represents individual mouse. Data combine three independent YUMMER1.7 and YUMM1.7 experiments. **G**, Averaged tumor growth of subcutaneous YUMMER1.7 melanomas in wild-type control ( $n = 6$ ; black) and *Angpt2<sup>ΔEC</sup>* ( $n = 6$ ; red) mice revealing significantly delayed tumor growth in *Angpt2<sup>ΔEC</sup>* mice. Data combine two independent experiments.  $P$  value for final time point as shown. Statistical analysis by Mann-Whitney test at day 25 after cell inoculation.

**Figure 5.**

CD8 $^{+}$  T cells mediate antitumor response to ANGPT2 inhibition in mouse melanoma. **A**, SCID (*C.B-*Igh-1 $b$* /lcrTac-*Prkdc*<sup>scid</sup>) mice deficient in B and T cells or C57BL/6 mice were inoculated with  $2.5 \times 10^5$  YUMMER1.7 cells and treated with anti-ANGPT2 (REGN910) or human IgG (REGN1945). SCID and C57BL/6 mice were administered anti-ANGPT2 every 3 days (4–5 total doses). C57BL/6 mice were treated with rat IgG or anti-CD8 $\alpha$  antibodies on days –2 and –1 prior to anti-ANGPT2 treatment start (day 0) and every 2 days following anti-ANGPT2 treatment start (eight total doses). **B**, Subcutaneous growth of YUMMER1.7 tumors in SCID mice following IgG or anti-ANGPT2 treatment (IgG,  $n = 7$ ; anti-ANGPT2,  $n = 7$ ). Each curve represents individual mouse. **C**, Quantification of cleaved-activated caspase-3 $^{+}$  percent area shows no difference in apoptosis in the tumor core after IgG or anti-ANGPT2 treatment in SCID mice. **D**, Comparison of tumor vascular leakage measured by extravasated fibrinogen from tumor vessels (CD31) in the periphery and core after IgG and anti-ANGPT2 treatment in SCID mice showing reduced vascular leakage after ANGPT2 blockade. Data combine two independent experiments. Error bars, SEM.  $P$  values as shown ( $P \geq 0.05$  not labeled). Statistical analysis by unpaired two-tailed Student  $t$  test. **E** and **F**, Comparison of YUMMER1.7 (IgG,  $n = 7$ ; anti-ANGPT2,  $n = 5$ ; anti-ANGPT2 plus anti-CD8 $\alpha$ ,  $n = 7$ ; **E**) and YUMMER1.7 (IgG,  $n = 5$ ; anti-ANGPT2,  $n = 6$ ; anti-ANGPT2 plus anti-CD8 $\alpha$ ,  $n = 6$ ; **F**) tumor growth after IgG or anti-ANGPT2 treatment with or without CD8 $^{+}$  T-cell depletion in C57BL/6 mice.  $P$  value for final time point as shown. Statistical analysis by ordinary one-way ANOVA with Tukey correction for multiple comparisons. **G**, Quantification of cleaved-activated caspase-3 $^{+}$  percent area reveals no difference in apoptosis in the tumor core after IgG- or anti-ANGPT2 plus anti-CD8-treated YUMMER1.7 mice. **H**, Quantification of vascular density (CD31) showing reduced vascular density after anti-ANGPT2 and anti-ANGPT2 plus anti-CD8 $\alpha$  compared with IgG-treated control. **I**, Reduced vascular leakage in the tumor periphery after anti-ANGPT2 and anti-ANGPT2 plus anti-CD8 $\alpha$  combination treatment compared with IgG treatment in YUMMER1.7 melanoma. For **C**, **D**, **G**, **H**, and **I**, each data point represents individual mouse. Data combine three independent experiments. Error bars, SEM.  $P$  values as shown ( $P \geq 0.05$  not labeled). Statistical analysis by ordinary one-way ANOVA with Tukey correction for multiple comparisons.*

(**Fig. 5A**). We confirmed complete depletion of CD8<sup>+</sup> T cells through immunofluorescence staining of tumor tissues showing no detectable CD8<sup>+</sup> T cells (Supplementary Fig. S12B). Consistent with the SCID experiment, concurrent depletion of CD8<sup>+</sup> T cells with ANGPT2 blockade abolished the antitumor effects of ANGPT2 inhibition, revealing YUMM1.7 and YUMMER1.7 tumor growth and apoptosis comparable with IgG-treated controls (**Fig. 5E** to **G**) despite decreased vascular density in the tumor and reduced vascular leakage at the tumor periphery (**Fig. 5H** and **I**). By corroborating studies in SCID mice, these data suggest that CD8<sup>+</sup> T cells play a major role in the antitumor response resulting from ANGPT2 blockade.

#### **Reversing T-cell exclusion by ANGPT2 inhibition enhances anti-PD-1 therapy efficacy**

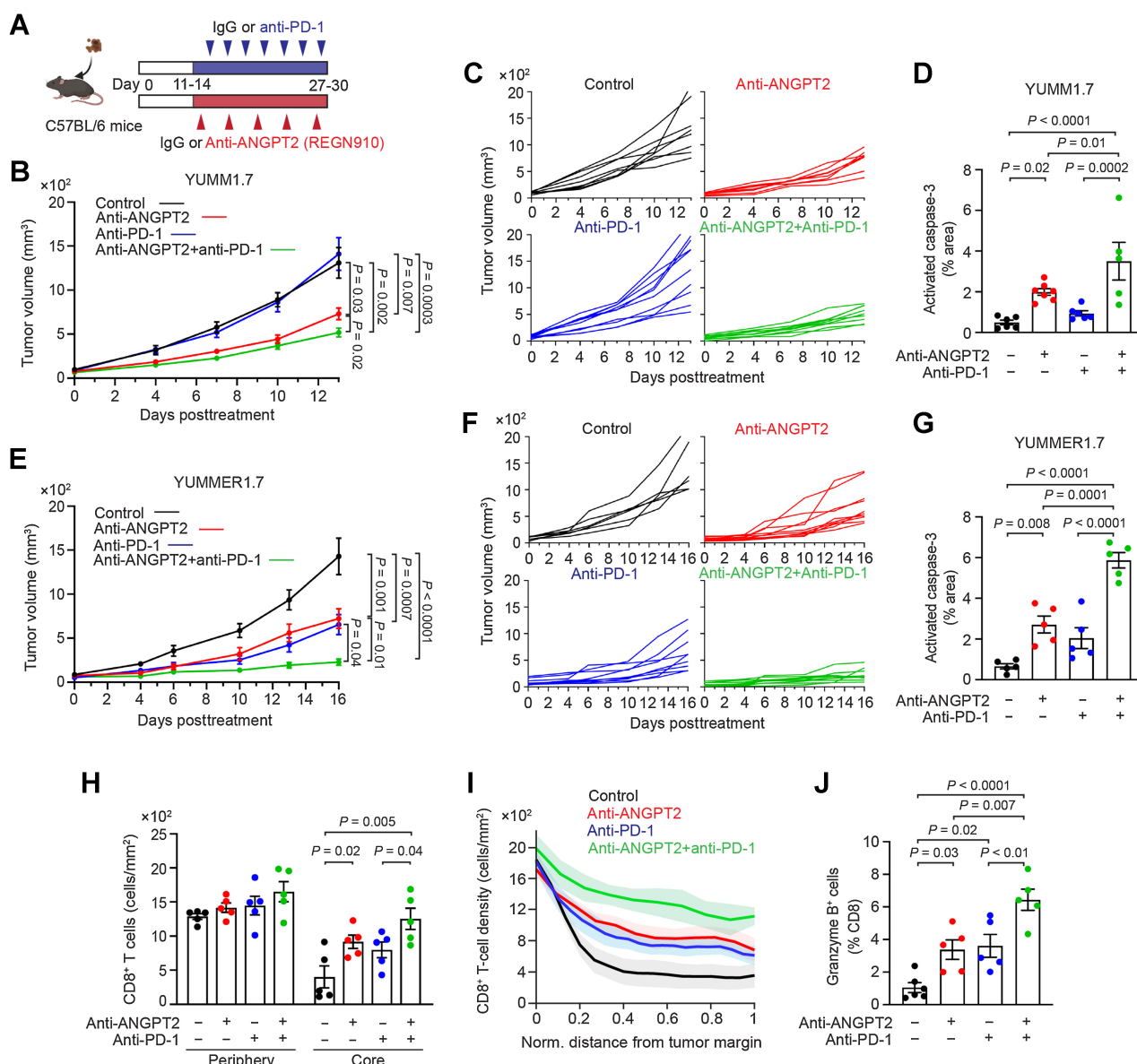
To determine if improved T-cell infiltration to the tumor core by ANGPT2 blockade can modulate response to checkpoint inhibitor therapy, we compared tumor progression after PD-1 inhibition with or without ANGPT2 blockade in the YUMM1.7 and YUMMER1.7 mouse models. Previous studies demonstrated that YUMMER1.7, but not the less immunogenic YUMM1.7, is sensitive to checkpoint inhibitors (34). For our studies, anti-ANGPT2 and anti-PD-1 antibodies were given alone or concurrently for 2 weeks (**Fig. 6A**). As expected, PD-1 inhibition alone showed resistance in YUMM1.7 tumors, which showed comparable tumor growth with IgG-treated controls ( $P = 0.95$ ; **Fig. 6B** and **C**). However, combination treatment with PD-1 inhibitor and ANGPT2 inhibitor in YUMM1.7 exhibited significantly improved antitumor effects compared with anti-PD-1 monotherapy ( $P = 0.0003$ ). Combination therapy also enhanced the antitumor response mediated by anti-ANGPT2 alone ( $P = 0.02$ ). Furthermore, consistent with previous findings (34), PD-1 inhibition itself slowed the rate of immunogenic YUMMER1.7 tumor growth compared with IgG-treated controls ( $P = 0.001$ ; **Fig. 6E** and **F**). The combination treatment of PD-1 inhibitor with ANGPT2 inhibitor enhanced antitumor effects compared with either monotherapy alone ( $P = 0.04$  for anti-PD-1 vs. combination and  $P = 0.01$  for anti-ANGPT2 vs. combination). Consistently, our data revealed significantly higher apoptosis in both YUMM1.7 and YUMMER1.7 tumors simultaneously targeted for ANGPT2 and PD-1 than in either monotherapy alone (**Fig. 6D** and **G**). The dual targeting of PD-1 and ANGPT2 further increased CD8<sup>+</sup> T-cell infiltration in the tumor core compared with monotherapies in YUMMER1.7 tumors (36% and 57% increases compared with anti-ANGPT2 alone and anti-PD-1 alone, respectively; **Fig. 6H**). However, the combination treatment did not significantly increase CD8<sup>+</sup> T-cell count in the tumor periphery. Analysis of CD8<sup>+</sup> T-cell abundance across whole tumor cross-sections showed the smallest spatial discrepancy in T-cell density between the tumor periphery and core after combination therapy compared with control and monotherapies (**Fig. 6I**). In addition, we found that either anti-PD-1 or anti-ANGPT2 alone increased the frequency of functional CD8<sup>+</sup> T cells measured by granzyme B expression compared with control YUMM1.7 tumors (**Fig. 6J**). The combination therapy with anti-PD-1 and anti-ANGPT2 showed even higher frequency of functional CD8<sup>+</sup> T cells compared with monotherapies. These findings suggest that ANGPT2 inhibition enhances anti-PD-1 therapy in both anti-PD-1-resistant and -responsive melanomas by improving T-cell infiltration to the tumor core. Collectively, our data suggest that ANGPT2 limits the efficacy of immunotherapy by inducing vascular destabilization at the tumor periphery to promote T-cell exclusion (**Fig. 7**).

## **Discussion**

In this study, our data demonstrated the regulation of ANGPT2-induced T-cell exclusion from the tumor core, highlighting ANGPT2/TIE2 signaling as a potential target to promote immune activation and enhance checkpoint inhibitor efficacy in melanoma. Specifically, we showed that (i) ANGPT2 upregulation and vascular destabilization in the tumor periphery are associated with T-cell exclusion from the tumor center in human and murine melanomas; (ii) genetic deletion and pharmacologic inhibition of ANGPT2 promote CD8<sup>+</sup> T-cell infiltration to the tumor core by improving vascular integrity preferentially at the tumor periphery, leading to delayed tumor growth in syngeneic murine melanomas; (iii) the absence of CD8<sup>+</sup> T cells counteracts antitumor effects following ANGPT2 neutralization; and (iv) ANGPT2 inhibition enhances the antitumor efficacy of anti-PD-1 therapy in both anti-PD-1-resistant and -responsive melanomas by reversing T-cell exclusion.

Clinical and preclinical studies have demonstrated beneficial antitumor effects when angiogenesis inhibitors are combined with checkpoint inhibitors (14, 30, 44–47). Current vascular modulators primarily target VEGF/VEGFR, which is a predominant angiogenic signaling pathway that promotes systemic and local immunosuppression (48–50). The combination of bevacizumab, a humanized mAb targeting VEGF, with checkpoint inhibitor therapy results in more favorable therapeutic outcomes in patients with melanoma than does checkpoint blockade alone (51). However, the emergence of resistance to anti-VEGF agents often results in metastatic recurrence and has thus limited therapeutic success. Preclinical studies have also shown that prolonged VEGF signaling inhibition can paradoxically fuel tumor progression and metastatic spread after initial treatment response (52, 53). Among compensatory proangiogenic signaling, ANGPT2/TIE signaling has been considered to be involved in anti-VEGF therapy resistance and consequent cancer progression, making this pathway a valuable target to overcome or reduce anti-VEGF resistance (43). Multiple ANGPT2-specific antibodies have been developed and are currently being tested in combination with other targeted therapies in clinical trials for patients with cancer (24). Of note, targeting ANGPT2 in combination with immune checkpoint inhibition is being tested in patients with advanced solid tumors including melanoma (phase I: NCT02141542 and NCT03239145). In addition, a recent study showed that acute pre-surgical ANGPT2 neutralization is sufficient to prolong mouse survival (54), emphasizing the importance of timed ANGPT2-targeted therapy for maximizing therapeutic efficacy.

T-cell exclusion from the tumor parenchyma is one of the mechanisms underlying immunosuppression in the TME and drives primary resistance to current immunotherapies (7, 8). Therefore, elucidating the biology that underpins this distinct pattern of T-cell exclusion is critical to identifying therapeutic targets and treatment strategies that will potentiate the antitumor immune response to current immunotherapies. Recent preclinical studies, including one from the De Palma group, have demonstrated that tumor vascular modulation driven by the concurrent neutralization of VEGF and ANGPT2 contributes to antitumor immunity (29, 30, 55). Our findings help define the mechanistic contributions of ANGPT2/TIE2 signaling to T-cell exclusion and tumor growth in melanomas of differing immunogenicity. Although previous studies have traditionally relied on B16 melanoma to study tumor vascular remodeling and treatment efficacy on the malignant growth of melanoma, B16 tumors do not recapitulate the relevant driver and somatic mutations that distinguish human melanoma as an immunogenic and aggressive cancer. We thus focused on using the YUMM1.7 and YUMMER1.7 melanoma cell lines, both of

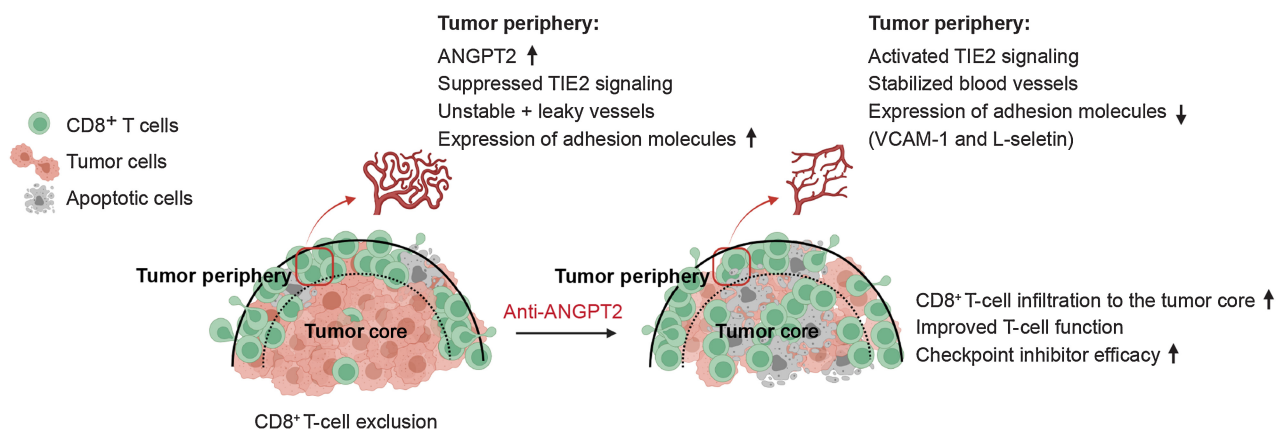


**Figure 6.**

**Figure 6.**  
**Reversing T-cell exclusion by ANGPT2 inhibition enhances anti-PD-1 therapy efficacy in mouse melanoma.** **A**, YUMMI.7 or YUMMER1.7 cells were subcutaneously inoculated in C57BL/6 mice and mice were treated with human (REGN1945) or rat IgG, anti-ANGPT2 (REGN910) or anti-PD-1 monotherapies, or combination (anti-ANGPT2 plus anti-PD-1) therapies. **B** and **C**, Averaged (**B**) and individual (**C**) growth of YUMMI.7 tumors in C57BL/6 mice following IgG, anti-ANGPT2, anti-PD-1, or anti-ANGPT2 plus anti-PD-1 treatment (IgG,  $n = 8$ ; anti-ANGPT2,  $n = 8$ ; anti-PD-1,  $n = 10$ ; anti-ANGPT2 plus anti-PD-1,  $n = 9$ ). **D**, Quantification showing greatest apoptosis (activated caspase-3) in tumor cores of YUMMI.7 mice treated with combination anti-ANGPT2 plus anti-PD-1 therapy. **E** and **F**, Averaged (**E**) and individual (**F**) growth of subcutaneous YUMMER1.7 tumors in C57BL/6 mice following IgG, anti-ANGPT2, anti-PD-1, or anti-ANGPT2 plus anti-PD-1 treatment (IgG,  $n = 6$ ; anti-ANGPT2,  $n = 10$ ; anti-PD-1,  $n = 9$ ; anti-ANGPT2 plus anti-PD-1,  $n = 10$ ). **G**, Quantification comparing apoptosis in YUMMER1.7 tumor cores of mice after indicated treatments. **H** and **I**, Quantification showing CD8<sup>+</sup> T-cell count in the tumor periphery and core (**H**) and CD8<sup>+</sup> T-cell density normalized by distance from the tumor margin (**I**) in YUMMER1.7 tumors after IgG, anti-ANGPT2, anti-PD-1, or anti-ANGPT2 plus anti-PD-1 treatment. **J**, Comparison of functional CD8<sup>+</sup> T-cell population (granzyme B<sup>+</sup>) in YUMMI.7 tumors after IgG, anti-ANGPT2, anti-PD-1, or anti-ANGPT2 plus anti-PD-1 treatment. For **D**, **G**, **H**, and **J**, each data point represents individual mouse. Error bars, SEM.  $P$  values as shown ( $P \geq 0.05$  not labeled). Statistical analysis by ordinary one-way ANOVA with Tukey correction for multiple corrections.

which harbor *Braf*, *Pten*, and *Cdkn2a* driver mutations, for comprehensive spatial analysis of CD8<sup>+</sup> T-cell distribution within the tumors. Among the key findings of this study was the preferential vascular stabilization in the tumor periphery and improved CD8<sup>+</sup> T-cell infiltration to the tumor core following pharmacologic or genetic

targeting of ANGPT2 in both YUMM1.7 and YUMMER1.7 melanomas. This is clinically important because the density of tumor-infiltrating CD8<sup>+</sup> T cells is one of the reliable predictors of response to checkpoint inhibitors (56, 57). Interestingly, we found heterogeneity in T-cell position in the tumor core after ANGPT2 blockade, as certain

**Figure 7.**

Model depicting the role of ANGPT2 in T-cell exclusion, limiting anti-PD-1 efficacy. ANGPT2 promotes vascular destabilization at the tumor periphery and restricts T-cell entry to the tumor core, thereby limiting tumor control and anti-PD-1 efficacy. Our study suggests ANGPT2 blockade enhances checkpoint inhibitor therapy by reversing T-cell exclusion in melanoma. (Created with BioRender.com.)

regions of the tumor showed more enriched T-cell density than others. Although not linked to tumor necrosis, further investigation is required to understand the regulation of specific T-cell position within the tumor. A previous study reported that the low somatic mutation burden in YUMM1.7 cells results in limited tumor immune responses represented by low T-cell infiltration, and that YUMM1.7 consequently exhibits similar growth in the presence and absence of a functional adaptive immune system (35). However, YUMMER1.7 derived from UVB irradiation and clonal selection of YUMM1.7 elicits a robust immune response due to increased somatic mutation burden and possibly more immunogenic neoantigens (34). Given the nature of parental YUMM1.7 tumors resistant to checkpoint inhibitor therapy, our data regarding YUMM1.7 melanoma suggests that targeting ANGPT2 can potentially render nonresponsive tumors susceptible. Furthermore, our findings in YUMMER1.7, which is highly immunogenic and responsive to checkpoint inhibitor treatment, suggest that targeting ANGPT2 can enhance the efficacy of checkpoint inhibitor therapy in responsive melanoma patients. Our data demonstrate that ANGPT2 inhibition also improves T-cell function in tumors, which could enhance checkpoint inhibitor therapy.

Our work continues to build upon previous findings regarding the role of ANGPT2, which is also known to control cytokine-induced vascular leakage (58), in vascular destabilization, and has unique implications in ANGPT2 regulation of T-cell exclusion through spatial vascular changes in tumors. As a mechanism, our results suggest that higher expression of adhesion molecules on endothelial cells at the tumor periphery might contribute to the preferential entry of T cells into the tissue at the tumor periphery rather than the tumor center. Consistent with previous studies demonstrating that ANGPT2 modulates the expression of endothelial cell adhesion molecules (59), our data show reduced endothelial expression of adhesion molecules in the tumor periphery after anti-ANGPT2 treatment, reducing the spatial discrepancy in adhesion molecule expression between the tumor periphery and core, which might improve T-cell access to the tumor core. Although earlier tumor xenograft studies in immunodeficient mice demonstrated antitumor efficacy of ANGPT2 inhibition in mice (38, 60), our results from immunodeficient and CD8<sup>+</sup> T-cell-depleted mice suggest that the immune system, particularly CD8<sup>+</sup> T cells, may serve as a primary determinant for antitumor efficacy by anti-ANGPT2 under certain conditions. Although our study did not

focus on the contribution of CD4<sup>+</sup> T cells to antitumor efficacy after targeting ANGPT2, it is possible that CD4<sup>+</sup> T cells play a partial and complementary role in CD8<sup>+</sup> T-cell-mediated antitumor action under ANGPT2 inhibition. In addition, given the different TMEs associated with primary and metastatic tumors, including their immunologic properties (61, 62), further investigation is required to fully understand our findings in the context of metastatic disease.

Although it is known that ANGPT2 is largely produced by endothelial cells (22), some studies have also reported low levels of ANGPT2 expression by tumor cells (18, 63). Interestingly, a recent study showed that tumor cell-derived ANGPT2 had no effect on vascular or immune function while promoting the metastatic progression of B16 melanoma (64). Our studies in YUMM1.7 and YUMMER1.7 tumors show predominant endothelial ANGPT2 expression, which modulates both vascular function and immune infiltration, also supported by the human melanoma single-cell RNA-seq dataset used for our study (GSE115978). The distinct contribution of ANGPT2 derived from different cells to tumor immune modulation deserves further study. Although our study did not investigate ANGPT1 levels during treatment, based on our findings revealing enhanced phosphorylated TIE2 after ANGPT2 inhibition, a decreased ANGPT2/ANGPT1 ratio, an indicator of vascular stability, is expected following anti-ANGPT2 treatment in our experimental models. Furthermore, our data demonstrated spatial FOXO1 activation at the tumor periphery, which could promote endothelial ANGPT2 expression in a positive feedback loop (39). Considering that hypoxia is another well-known regulator for ANGPT2 expression (65, 66), hypoxia-inducible factors could also regulate ANGPT2 expression in the tumor core, where vascular density is low.

Although this study supports the indirect effects of ANGPT2 on immune evasion by vascular destabilization, it is possible that ANGPT2 promotes tumor progression through direct effects on immune cells. Previous studies have shown that ANGPT2 enhances the recruitment of TEMs, which have angiogenic and immunosuppressive functions (67–69). However, a recent study using multiple preclinical tumor models and meta-analysis of RNA-seq data reported a dispensable role of TEMs in tumor angiogenesis, metastasis, and tumor recurrence after chemotherapy, challenging the previously reported role of TEMs (70). For our FACS analyses, we defined TEM population by referring to previous studies

(F4/80<sup>+</sup>CD11b<sup>+</sup>Ly6C<sup>-</sup>Ly6G<sup>-</sup>CD11c<sup>-</sup>CD206<sup>+</sup>; ref. 29) but also observed a small subset of macrophages with TIE2 expression (~0.36% of CD45<sup>+</sup> cells) in YUMMER1.7 tumors. Contrasting CD8<sup>+</sup> T-cell findings, our study demonstrated a less evident exclusion pattern of immunosuppressive myeloid cells such as TAMs and MDSCs, whose frequencies in tumors were not significantly changed after ANGPT2 inhibition, except for PMN-MDSCs. Nevertheless, our data suggest other tumor immunosuppressive actions of ANGPT2, as evidenced by an increased M1/M2 TAM ratio and reduced frequency of Tregs in the tumor core following ANGPT2 blockade. It is also noteworthy that basal TIE2 expression in the tumor vasculature was low in the melanomas we studied, similar to the phenotype of endothelial tip cells with TIE2 downregulation (71, 72).

In summary, this study establishes the mechanistic role of ANGPT2/TIE2 signaling in T-cell exclusion and efficacy of anti-PD-1 therapy in melanomas with distinct patterns of immunogenicity (Fig. 7). Importantly, a recent clinical trial in hepatocellular carcinoma has shown promising results after combined antiangiogenic and checkpoint inhibitor treatment (73). Furthermore, another phase I clinical study exhibited a reasonable safety profile when patients with melanoma received anti-CTLA4 in combination with ANGPT2 inhibition (MEDI3617; ref. 74), which warrants further investigation into the underlying mechanism of action to properly rationalize combination therapy in different tumors. Our work focusing on the spatial vascular regulation of T-cell exclusion from the tumor core in melanoma has clinical significance for suppressing tumor progression and potentially enhancing immune checkpoint inhibitor efficacy for patients with cancer, especially for those harboring tumors with poor immune cell infiltration and resistance to current immunotherapies.

### Authors' Disclosures

C.J. Shawber reports grants from Department of Defense, NIH, and Lymphatic Malformation Institute outside the submitted work. R.D. Carvajal reports personal fees from Alkermes, BMS, Castle Biosciences, Delcath, Eisai, Hengrui, Ideaya, Immunocore, InxMed, Iovance, Merck, Novartis, Oncosec, Pierre Fabre, PureTech Health, Regeneron, Sanofi Genzyme, Sorrento Therapeutics, and TriSalus outside the submitted work. G. Thurston reports employment by Regeneron Pharmaceuticals and ownership of Regeneron Pharmaceuticals stock. J. An reports grants from National Research Foundation of Korea during the conduct of the study. A.W. Lund

reports consulting services for AGS Therapeutics. No disclosures were reported by the other authors.

### Authors' Contributions

**H.-R. Park:** Conceptualization, data curation, formal analysis, validation, writing–review and editing. **A. Shiva:** Conceptualization, data curation, formal analysis, validation, writing–review and editing. **P. Cummings:** Validation, investigation. **S. Kim:** Data curation, formal analysis. **S. Kim:** Validation, investigation. **E. Lee:** Validation, investigation. **A. Leong:** Investigation. **S. Chowdhury:** Investigation. **C. Shawber:** Resources. **R. Carvajal:** Resources, data curation. **G. Thurston:** Resources. **J.-Y. An:** Data curation, formal analysis. **A.W. Lund:** Resources, methodology. **H.W. Yang:** Data curation, software, formal analysis, methodology, writing–review and editing. **M. Kim:** Conceptualization, data curation, formal analysis, supervision, funding acquisition, investigation, writing–original draft, writing–review and editing.

### Acknowledgments

The authors thank Dr. Gou Young Koh (Korea Advanced Institute of Science and Technology) for providing the *Angpt2*<sup>flox/flox</sup> mice and Dr. Ralf Adams (Max Planck Institute) for providing the VE-cadherin-CreER<sup>T2</sup> mice. They thank Sophie O'Keefe (Columbia University Irving Medical Center) for reviewing the manuscript. The authors also thank Michael Kissner, Director of Operations of Columbia Stem Cell Initiative Flow Cytometry Core Facility, for assistance and technical advice with flow cytometry, the DataBase Shared Resource at HICCC for screening tissues samples of patients with melanoma, and the Molecular Pathology Shared Resource at HICCC for providing human melanoma tissues and pathological analyses. This work was supported by the Melanoma Research Foundation (to M. Kim and H. Yang), the Neuroendocrine Research Foundation (855538 to M. Kim), the NIH/NCI (R37-CA266270 to M. Kim), the American Cancer Society (RSG-22-167-01-MM to M. Kim and RSG-22-101-01-CDP to H. Yang), the HICCC (P30-CA013696 to M. Kim), and the National Research Foundation of Korea (NRF-2021R1A4A1029097 and NRF-2019M3E5D3073568 to J. An).

The publication costs of this article were defrayed in part by the payment of publication fees. Therefore, and solely to indicate this fact, this article is hereby marked "advertisement" in accordance with 18 USC section 1734.

### Note

Supplementary data for this article are available at Cancer Research Online (<http://cancerres.aacrjournals.org/>).

Received September 6, 2022; revised January 13, 2023; accepted April 18, 2023; published first April 24, 2023.

### References

- Schadendorf D, van Akkooi ACJ, Berking C, Griewank KG, Gutzmer R, Hauschild A, et al. Melanoma. *Lancet* 2018;392:971–84.
- Passarelli A, Mannavola F, Stucci LS, Tucci M, Silvestris F. Immune system and melanoma biology: a balance between immunosurveillance and immune escape. *Oncotarget* 2017;8:106132–42.
- Postow MA, Chesney J, Pavlick AC, Robert C, Grossmann K, McDermott D, et al. Nivolumab and ipilimumab versus ipilimumab in untreated melanoma. *N Engl J Med* 2015;372:2006–17.
- Robert C, Schachter J, Long GV, Arance A, Grob JJ, Mortier L, et al. Pembrolizumab versus ipilimumab in advanced melanoma. *N Engl J Med* 2015;372:2521–32.
- Wolchok JD, Chiarion-Sileni V, Gonzalez R, Rutkowski P, Grob JJ, Cowey CL, et al. Overall survival with combined nivolumab and ipilimumab in advanced melanoma. *N Engl J Med* 2017;377:1345–56.
- Atkins MB, Curiel-Lewandrowski C, Fisher DE, Swetter SM, Tsao H, Aguirre-Ghiso JA, et al. The state of melanoma: emergent challenges and opportunities. *Clin Cancer Res* 2021;27:2678–97.
- Mariathasan S, Turley SJ, Nickles D, Castiglioni A, Yuen K, Wang Y, et al. TGFbeta attenuates tumour response to PD-L1 blockade by contributing to exclusion of T cells. *Nature* 2018;554:544–8.
- Joyce JA, Fearon DT. T cell exclusion, immune privilege, and the tumor microenvironment. *Science* 2015;348:74–80.
- Feig C, Jones JO, Kraman M, Wells RJ, Deonarine A, Chan DS, et al. Targeting CXCL12 from FAP-expressing carcinoma-associated fibroblasts synergizes with anti-PD-L1 immunotherapy in pancreatic cancer. *Proc Natl Acad Sci U S A* 2013;110:20212–7.
- Kim JM, Chen DS. Immune escape to PD-L1/PD-1 blockade: seven steps to success (or failure). *Ann Oncol* 2016;27:1492–504.
- Hurwitz H, Fehrenbacher L, Novotny W, Cartwright T, Hainsworth J, Heim W, et al. Bevacizumab plus irinotecan, fluorouracil, and leucovorin for metastatic colorectal cancer. *N Engl J Med* 2004;350:2335–42.
- Tong RT, Boucher Y, Kozin SV, Winkler F, Hicklin DJ, Jain RK. Vascular normalization by vascular endothelial growth factor receptor 2 blockade induces a pressure gradient across the vasculature and improves drug penetration in tumors. *Cancer Res* 2004;64:3731–6.
- Shrimali RK, Yu Z, Theoret MR, Chinnasamy D, Restifo NP, Rosenberg SA. Antiangiogenic agents can increase lymphocyte infiltration into tumor and enhance the effectiveness of adoptive immunotherapy of cancer. *Cancer Res* 2010;70:6171–80.
- Fukumura D, Kloepper J, Amoozgar Z, Duda DG, Jain RK. Enhancing cancer immunotherapy using antiangiogenics: opportunities and challenges. *Nat Rev Clin Oncol* 2018;15:325–40.
- Khan KA, Kerbel RS. Improving immunotherapy outcomes with anti-angiogenic treatments and vice versa. *Nat Rev Clin Oncol* 2018;15:310–24.

16. Etoh T, Inoue H, Tanaka S, Barnard GF, Kitano S, Mori M. Angiopoietin-2 is related to tumor angiogenesis in gastric carcinoma: possible *in vivo* regulation via induction of proteases. *Cancer Res* 2001;61:2145–53.
17. Ochiimi T, Tanaka S, Oka S, Hiyama T, Ito M, Kitadai Y, et al. Clinical significance of angiopoietin-2 expression at the deepest invasive tumor site of advanced colorectal carcinoma. *Int J Oncol* 2004;24:539–47.
18. Sfiligoi C, de Luca A, Cascone I, Sorbello V, Fuso L, Ponzone R, et al. Angiopoietin-2 expression in breast cancer correlates with lymph node invasion and short survival. *Int J Cancer* 2003;103:466–74.
19. Brunet A, Bonni A, Zigmond MJ, Lin MZ, Juo P, Hu LS, et al. Akt promotes cell survival by phosphorylating and inhibiting a Forkhead transcription factor. *Cell* 1999;96:857–68.
20. Daly C, Wong V, Burova E, Wei Y, Zabski S, Griffiths J, et al. Angiopoietin-1 modulates endothelial cell function and gene expression via the transcription factor FKHR (FOXO1). *Genes Dev* 2004;18:1060–71.
21. Kim I, Kim HG, So JN, Kim JH, Kwak HJ, Koh GY. Angiopoietin-1 regulates endothelial cell survival through the phosphatidylinositol 3'-Kinase/Akt signal transduction pathway. *Circ Res* 2000;86:24–9.
22. Augustin HG, Koh GY, Thurston G, Alitalo K. Control of vascular morphogenesis and homeostasis through the angiopoietin-Tie system. *Nat Rev Mol Cell Biol* 2009;10:165–77.
23. Bogdanovic E, Nguyen VP, Dumont DJ. Activation of Tie2 by angiopoietin-1 and angiopoietin-2 results in their release and receptor internalization. *J Cell Sci* 2006;119:3551–60.
24. Leong A, Kim M. The angiopoietin-2 and TIE pathway as a therapeutic target for enhancing antiangiogenic therapy and immunotherapy in patients with advanced cancer. *Int J Mol Sci* 2020;21:8689.
25. Maisonpierre PC, Suri C, Jones PF, Bartunkova S, Wiegand SJ, Radziejewski C, et al. Angiopoietin-2, a natural antagonist for Tie2 that disrupts in vivo angiogenesis. *Science* 1997;277:55–60.
26. Yancopoulos GD, Davis S, Gale NW, Rudge JS, Wiegand SJ, Holash J. Vascular-specific growth factors and blood vessel formation. *Nature* 2000;407:242–8.
27. Thurston G, Daly C. The complex role of angiopoietin-2 in the angiopoietin-tie signaling pathway. *Cold Spring Harb Perspect Med* 2012;2:a006550.
28. Ghosh CC, Thamm K, Bergelli AV, Schrimpf C, Maski MR, Abid T, et al. Drug repurposing screen identifies Foxo1-dependent angiopoietin-2 regulation in sepsis. *Crit Care Med* 2015;43:e230–40.
29. Mazzieri R, Pucci F, Moi D, Zonari E, Ranghetti A, Berti A, et al. Targeting the ANG2/TIE2 axis inhibits tumor growth and metastasis by impairing angiogenesis and disabling rebounds of proangiogenic myeloid cells. *Cancer Cell* 2011;19:512–26.
30. Schmittnaegel M, Rigamonti N, Kadioglu E, Cassará A, Wyser Rmili C, Kialainen A, et al. Dual angiopoietin-2 and VEGFA inhibition elicits antitumor immunity that is enhanced by PD-1 checkpoint blockade. *Sci Transl Med* 2017;9:eaak9670.
31. Lee SJ, Lee CK, Kang S, Park I, Kim YH, Kim SK, et al. Angiopoietin-2 exacerbates cardiac hypoxia and inflammation after myocardial infarction. *J Clin Invest* 2018;128:5018–33.
32. Shen B, Shang Z, Wang B, Zhang L, Zhou F, Li T, et al. Genetic dissection of tie pathway in mouse lymphatic maturation and valve development. *Arterioscler Thromb Vasc Biol* 2014;34:1221–30.
33. Sorensen I, Adams RH, Gossler A. DLL1-mediated Notch activation regulates endothelial identity in mouse fetal arteries. *Blood* 2009;113:5680–8.
34. Wang J, Perry CJ, Meeth K, Thakral D, Damsky W, Micevic G, et al. UV-induced somatic mutations elicit a functional T cell response in the YUMMER1.7 mouse melanoma model. *Pigment Cell Melanoma Res* 2017;30:428–35.
35. Meeth K, Wang JX, Micevic G, Damsky W, Bosenberg MW. The YUMM lines: a series of congenic mouse melanoma cell lines with defined genetic alterations. *Pigment Cell Melanoma Res* 2016;29:590–7.
36. Steele MM, Jaiswal A, Delclaux I, Dryg ID, Murugan D, Femel J, et al. T cell egress via lymphatic vessels is tuned by antigen encounter and limits tumor control. *Nat Immunol* 2023;24:664–75.
37. Jerby-Arnon L, Shah P, Cuoco MS, Rodman C, Su MJ, Melms JC, et al. A cancer cell program promotes T cell exclusion and resistance to checkpoint blockade. *Cell* 2018;175:984–97.
38. Daly C, Eichten A, Castanaro C, Pasnikowski E, Adler A, Lalani AS, et al. Angiopoietin-2 functions as a Tie2 agonist in tumor models, where it limits the effects of VEGF inhibition. *Cancer Res* 2013;73:108–18.
39. Kim M, Allen B, Korhonen EA, Nitschke M, Yang HW, Baluk P, et al. Opposing actions of angiopoietin-2 on Tie2 signaling and FOXO1 activation. *J Clin Invest* 2016;126:3511–25.
40. Potente M, Urbich C, Sasaki K, Hofmann WK, Heeschen C, Aicher A, et al. Involvement of Foxo transcription factors in angiogenesis and postnatal neovascularization. *J Clin Invest* 2005;115:2382–92.
41. Cancer Genome Atlas N. Genomic classification of cutaneous melanoma. *Cell* 2015;161:1681–96.
42. Mantovani A, Sozzani S, Locati M, Allavena P, Sica A. Macrophage polarization: tumor-associated macrophages as a paradigm for polarized M2 mononuclear phagocytes. *Trends Immunol* 2002;23:549–55.
43. Rigamonti N, Kadioglu E, Keklikoglu I, Wyser Rmili C, Lew CC, De Palma M. Role of angiopoietin-2 in adaptive tumor resistance to VEGF signaling blockade. *Cell Rep* 2014;8:696–706.
44. Ott PA, Hodi FS, Buchbinder EI. Inhibition of immune checkpoints and vascular endothelial growth factor as combination therapy for metastatic melanoma: an overview of rationale, preclinical evidence, and initial clinical data. *Front Oncol* 2015;5:202.
45. Seidel JA, Otsuka A, Kabashima K. Anti-PD-1 and anti-CTLA-4 therapies in cancer: mechanisms of action, efficacy, and limitations. *Front Oncol* 2018;8:86.
46. Sharma P, Hu-Lieskovian S, Wargo JA. Primary, adaptive, and acquired resistance to cancer immunotherapy. *Cell* 2017;168:707–23.
47. Yasuda S, Sho M, Yamato I, Yoshiji H, Wakatsuki K, Nishiwada S, et al. Simultaneous blockade of programmed death 1 and vascular endothelial growth factor receptor 2 (VEGFR2) induces synergistic anti-tumour effect *in vivo*. *Clin Exp Immunol* 2013;172:500–6.
48. Huang Y, Goel S, Duda DG, Fukumura D, Jain RK. Vascular normalization as an emerging strategy to enhance cancer immunotherapy. *Cancer Res* 2013;73:2943–8.
49. Jain RK. Antiangiogenesis strategies revisited: from starving tumors to alleviating hypoxia. *Cancer Cell* 2014;26:605–22.
50. Voron T, Colussi O, Marcheteau E, Pernot S, Nizard M, Pointet AL, et al. VEGF-A modulates expression of inhibitory checkpoints on CD8+ T cells in tumors. *J Exp Med* 2015;212:139–48.
51. Hodi FS, Lawrence D, Lezcano C, Wu X, Zhou J, Sasada T, et al. Bevacizumab plus ipilimumab in patients with metastatic melanoma. *Cancer Immunol Res* 2014;2:632–42.
52. Casanovas O, Hicklin DJ, Bergers G, Hanahan D. Drug resistance by evasion of antiangiogenic targeting of VEGF signaling in late-stage pancreatic islet tumors. *Cancer Cell* 2005;8:299–309.
53. Ebos JM, Lee CR, Cruz-Munoz W, Bjarnason GA, Christensen JG, Kerbel RS. Accelerated metastasis after short-term treatment with a potent inhibitor of tumor angiogenesis. *Cancer Cell* 2009;15:232–9.
54. Gengenbacher N, Singhal M, Mogler C, Hai L, Milde L, Pari AAA, et al. Timed Ang2-targeted therapy identifies the angiopoietin-Tie pathway as key regulator of fatal lymphogenous metastasis. *Cancer Discov* 2021;11:424–45.
55. Kashyap AS, Schmittnaegel M, Rigamonti N, Pais-Ferreira D, Mueller P, Buchi M, et al. Optimized antiangiogenic reprogramming of the tumor microenvironment potentiates CD40 immunotherapy. *Proc Natl Acad Sci U S A* 2020;117:541–51.
56. Tumeh PC, Harview CL, Yearley JH, Shintaku IP, Taylor EJ, Robert L, et al. PD-1 blockade induces responses by inhibiting adaptive immune resistance. *Nature* 2014;515:568–71.
57. Fridman WH, Pages F, Sautes-Fridman C, Galon J. The immune contexture in human tumours: impact on clinical outcome. *Nat Rev Cancer* 2012;12:298–306.
58. Benest AV, Kruse K, Savant S, Thomas M, Laib AM, Loos EK, et al. Angiopoietin-2 is critical for cytokine-induced vascular leakage. *PLoS One* 2013;8:e70459.
59. Fiedler U, Reiss Y, Scharpfenecker M, Grunow V, Koidl S, Thurston G, et al. Angiopoietin-2 sensitizes endothelial cells to TNF-alpha and has a crucial role in the induction of inflammation. *Nat Med* 2006;12:235–9.
60. Oliner J, Min H, Leal J, Yu D, Rao S, You E, et al. Suppression of angiogenesis and tumor growth by selective inhibition of angiopoietin-2. *Cancer Cell* 2004;6:507–16.
61. Cacho-Diaz B, Garcia-Botello DR, Wegman-Ostrosky T, Reyes-Soto G, Ortiz-Sanchez E, Herrera-Montalvo LA. Tumor microenvironment differences between primary tumor and brain metastases. *J Transl Med* 2020;18:1.
62. Zarrilli G, Businello G, Dieci MV, Paccagnella S, Carraro V, Cappellessi R, et al. The tumor microenvironment of primitive and metastatic breast cancer: implications for novel therapeutic strategies. *Int J Mol Sci* 2020;21:8102.
63. Gu J, Yamamoto H, Ogawa M, Ngan CY, Danno K, Hemmi H, et al. Hypoxia-induced up-regulation of angiopoietin-2 in colorectal cancer. *Oncol Rep* 2006;15:779–83.
64. Abdul Pari AA, Singhal M, Hubers C, Mogler C, Schieb B, Gampp A, et al. Tumor cell-derived angiopoietin-2 promotes metastasis in melanoma. *Cancer Res* 2020;80:2586–98.

65. Pichiule P, Chavez JC, LaManna JC. Hypoxic regulation of angiopoietin-2 expression in endothelial cells. *J Biol Chem* 2004;279:12171–80.
66. Simon MP, Tournaire R, Pouyssegur J. The angiopoietin-2 gene of endothelial cells is up-regulated in hypoxia by a HIF binding site located in its first intron and by the central factors GATA-2 and Ets-1. *J Cell Physiol* 2008;217:809–18.
67. Coffelt SB, Tal AO, Scholz A, De Palma M, Patel S, Urbich C, et al. Angiopoietin-2 regulates gene expression in TIE2-expressing monocytes and augments their inherent proangiogenic functions. *Cancer Res* 2010;70:5270–80.
68. Murdoch C, Tazzyman S, Webster S, Lewis CE. Expression of Tie-2 by human monocytes and their responses to angiopoietin-2. *J Immunol* 2007;178:7405–11.
69. Venneri MA, De Palma M, Ponzoni M, Pucci F, Scielzo C, Zonari E, et al. Identification of proangiogenic TIE2-expressing monocytes (TEMs) in human peripheral blood and cancer. *Blood* 2007;109:5276–85.
70. Jakab M, Rostalski T, Lee KH, Mogler C, Augustin HG. Tie2 receptor in tumor-infiltrating macrophages is dispensable for tumor angiogenesis and tumor relapse after chemotherapy. *Cancer Res* 2022;82:1353–64.
71. del Toro R, Prahl C, Mathivet T, Siegfried G, Kaminker JS, Larrivee B, et al. Identification and functional analysis of endothelial tip cell-enriched genes. *Blood* 2010;116:4025–33.
72. Felcht M, Luck R, Schering A, Seidel P, Srivastava K, Hu J, et al. Angiopoietin-2 differentially regulates angiogenesis through TIE2 and integrin signaling. *J Clin Invest* 2012;122:1991–2005.
73. Finn RS, Qin S, Ikeda M, Galle PR, Dureux M, Kim TY, et al. Atezolizumab plus bevacizumab in unresectable hepatocellular carcinoma. *N Engl J Med* 2020;382:1894–905.
74. Ott PA, Nazzaro M, Pfaff KL, Gjini E, Felt KD, Wolff JO, et al. Combining CTLA-4 and angiopoietin-2 blockade in patients with advanced melanoma: a phase I trial. *J Immunother Cancer* 2021;9:e003318.